FINAL REPORT

FOR

A DAY-NIGHT HIGH RESOLUTION INFRARED RADIOMETER EMPLOYING TWO-STAGE RADIANT COOLING

PART II

BREADBOARD DAY-NIGHT RADIOMETER

Contract No. NAS 5-10113

Prepared by

ITT Industrial Laboratories

Fort Wayne, Indiana 46803

For

National Aeronautics and Space Administration

Goddard Space Flight Center

Greenbelt, Maryland 20771

ITTIL No. 67-1064 28 December 1967

FINAL REPORT

FOR

A DAY-NIGHT HIGH RESOLUTION INFRARED RADIOMETER EMPLOYING TWO-STAGE RADIANT COOLING

PART II

BREADBOARD DAY-NIGHT RADIOMETER

Contract No. NAS 5-10113

Prepared by

ITT Industrial Laboratories
Fort Wayne, Indiana 46803

For

National Aeronautics and Space Administration
Goddard Space Flight Center
Greenbelt, Maryland 20771

Contributors

R. V. Annable, J. F. Lodder, D. J. Juarez,
W. H. Wallschlaeger, P. C. Murray

Approved by

K. L. DeBrosse, Manager Space & Applied Science Dept.	Dr. C. W. Steeg Jr., Director Product Development	Dr. R. T. Watson, President ITT Industrial Laboratories

ABSTRACT

This part of the final project report covers Phase III, the integration of the two-stage radiant cooler into a working breadboard model of a day-night radiometer. It describes the mechanical, optical, and electronic design of the radiometer. The characteristics of the infrared detector are given and the test instrumentation outlined. The radiometer operates in the 10.5 to 12.5 micron band and has a collecting aperture diameter of 4 inches. The mechanical drive and electronic bandwidth are designed for contiguous subpoint scanning at an altitude of 750 n mi and an instantaneous field-of-view of 2.5 mr on a side. The noise equivalent temperature is less than 170 degrees K, and the noise equivalent temperature difference at 220 degrees K is less than 2 degrees K.

Part I of the final project report covers Phase I, preliminary design study, and Phase II, two-stage radiant cooler.

TABLE OF CONTENTS

LIST OF ILLUSTRATIONS

LIST OF TABLES

1.0 OVERALL CHARACTERISTICS

The breadboard radiometer is shown in Figure 1, and its characteristics are given in Table 1. The components added to the two-stage radiant cooler to form the radiometer are the scan head (Section 2.0), relay optics (Section 3.0), infrared detector (Section 4.0), and radiometer electronics (Section 5.0). Electrical and thermal test instruments (Section 6.0) were used to measure the performance of the complete radiometer (Section 7.0).

Table 1

Overall Radiometer Characteristics

	Specified	Achieved
Spectral region (-6 db points)	10.5 to 12.5 microns, ± 0.1 micron	10.44 to 12.53 microns
Collecting aperture diameter	5 inches maximum	4 inches outside
Instantaneous field-of-view (-6 db points)	2.5 ± 0.2 mr x 2.5 ± 0.2 mr	2.6 mr x 2.2 mr
Noise equivalent temperature	Below 170°K	Below 160° K*
Noise equivalent temperature difference	Less than 2°K at 220°K	Less than 1°K* at 220°K
Chopping frequency and electronic bandwidth	For contiguous subpoint scanning from 750 n mi	6 khz and 2.47 khz

---

* Estimated

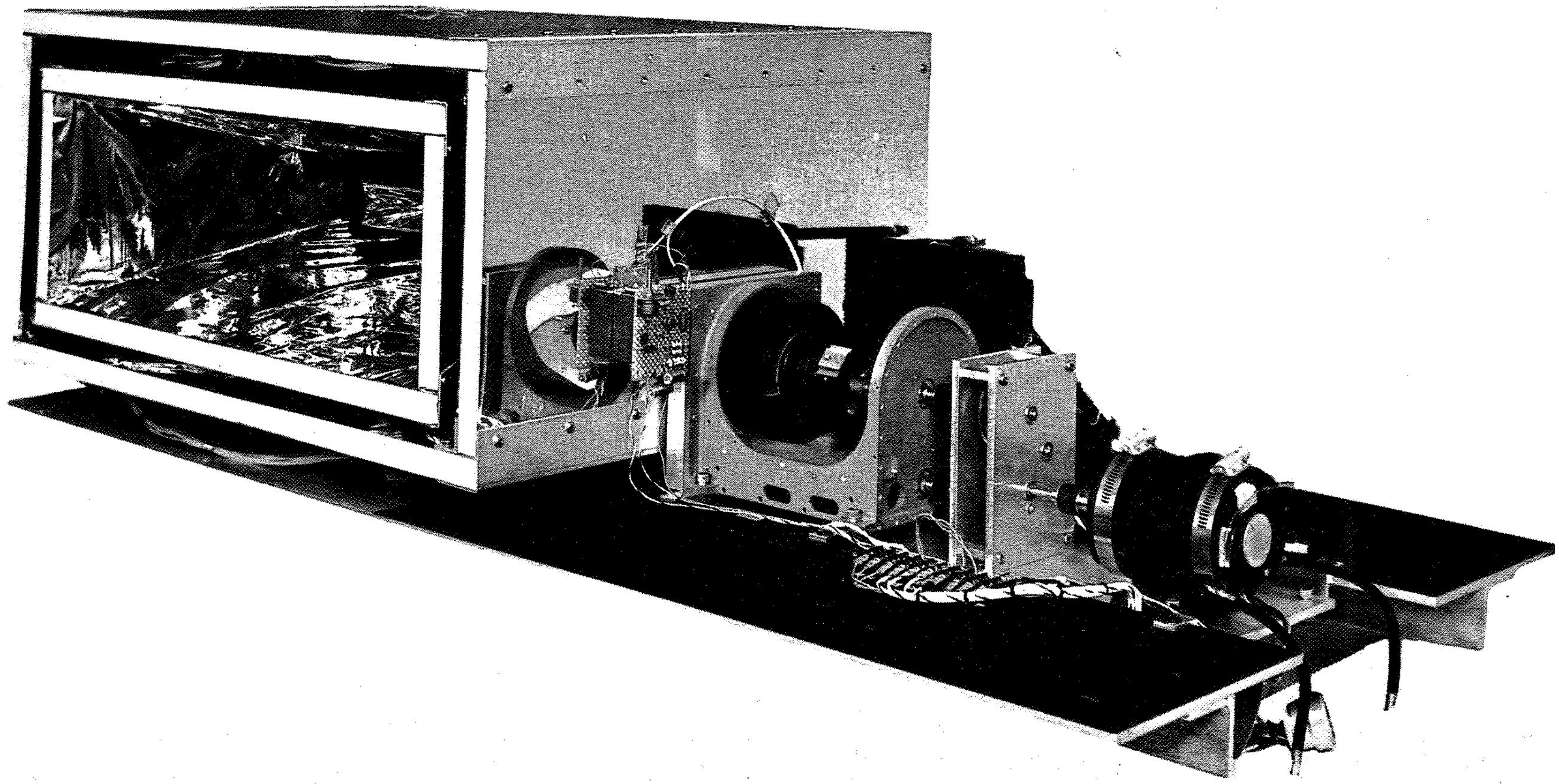

Figure 1 Breadboard Day-Night Radiometer

2.0 SCAN HEAD

The scan head of the breadboard radiometer is shown in Figure 2. It consists of a drive motor, gear box, casting, scanning mirror, primary telescope, and mechanical chopper. The drive motor is a Bodine model 246 lubricated with low vapor pressure silicone grease (General Electric Versilube G-300). The output of the gear box drives the scan mirror and chopper through flexible couplings; the gear train is shown in Figure 3. The casting (Figure 4) is made of KIA magnesium alloy that has been stress relieved after machining and surface treated with Dow 23. The scanning mirror and primary telescope are described in Section 3.0. The chopper disk is shown in Figure 5 and the chopper assembly in Figure 6.

For contiguous scan lines at the subpoint from an altitude of 750 n mi, the scan mirror must rotate at 100 rpm when the instantaneous field-of-view is 2.5 milliradians (Section 7.0). The electronic post-demodulation bandwidth is then 2100 hz. The chopping frequency must exceed twice this value; a rate of 6000 hz was selected. For a chopper with 180 teeth, the corresponding chopper wheel rotational rate is 2000 rpm.

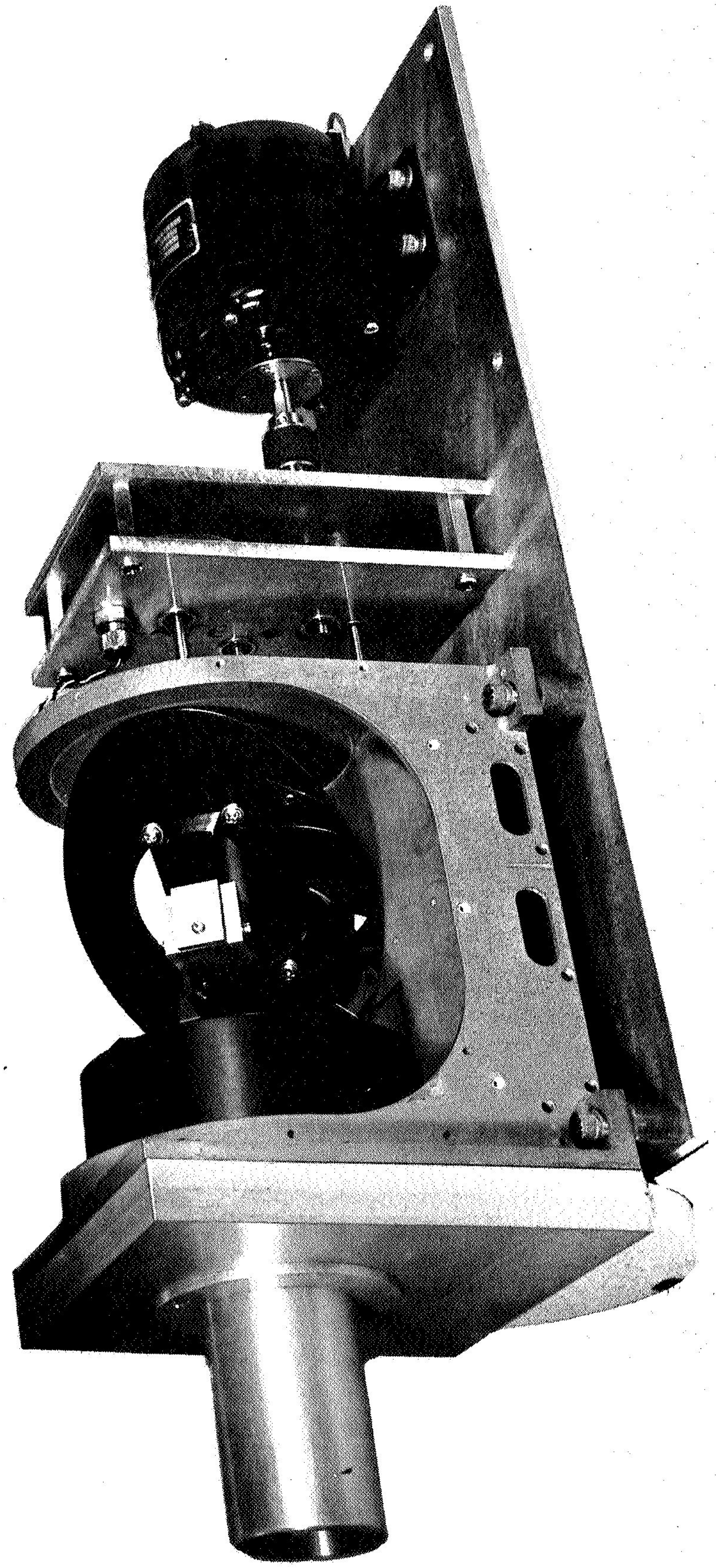

Figure 2 Radiometer Scan Head

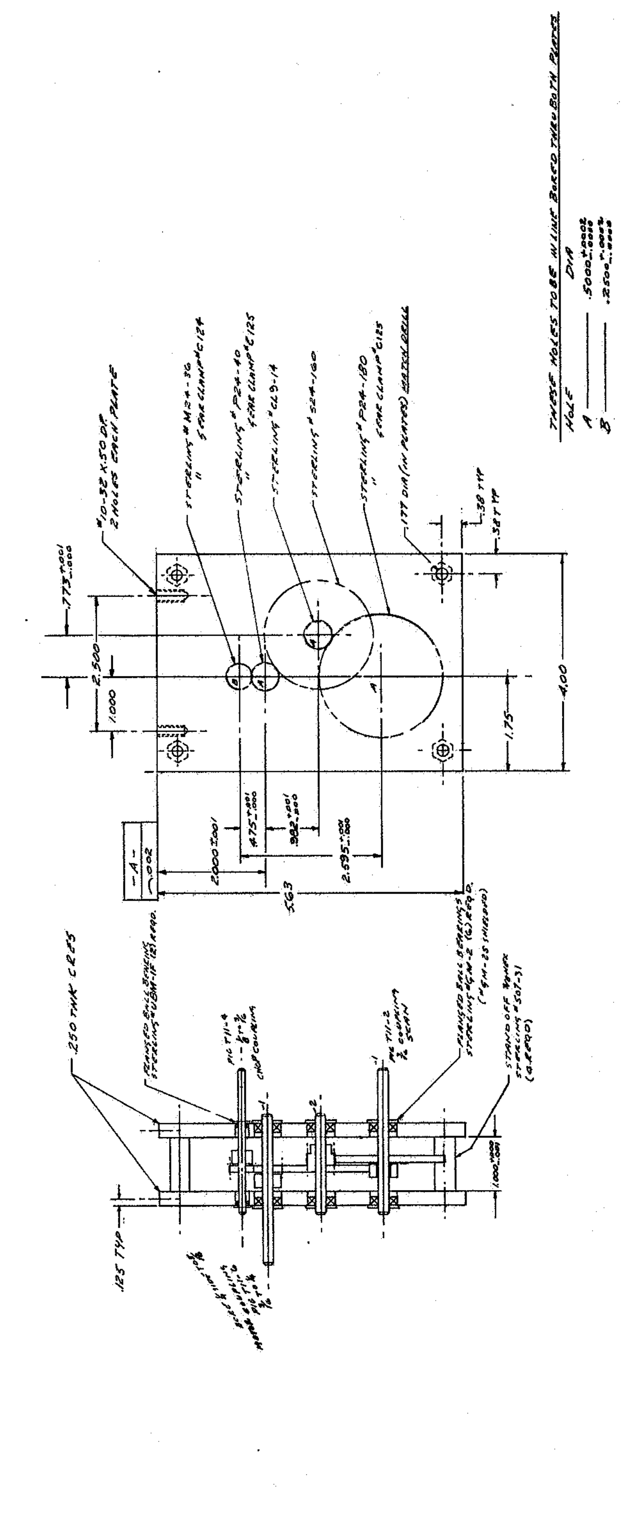

Figure 3 Radiometer Gear Train

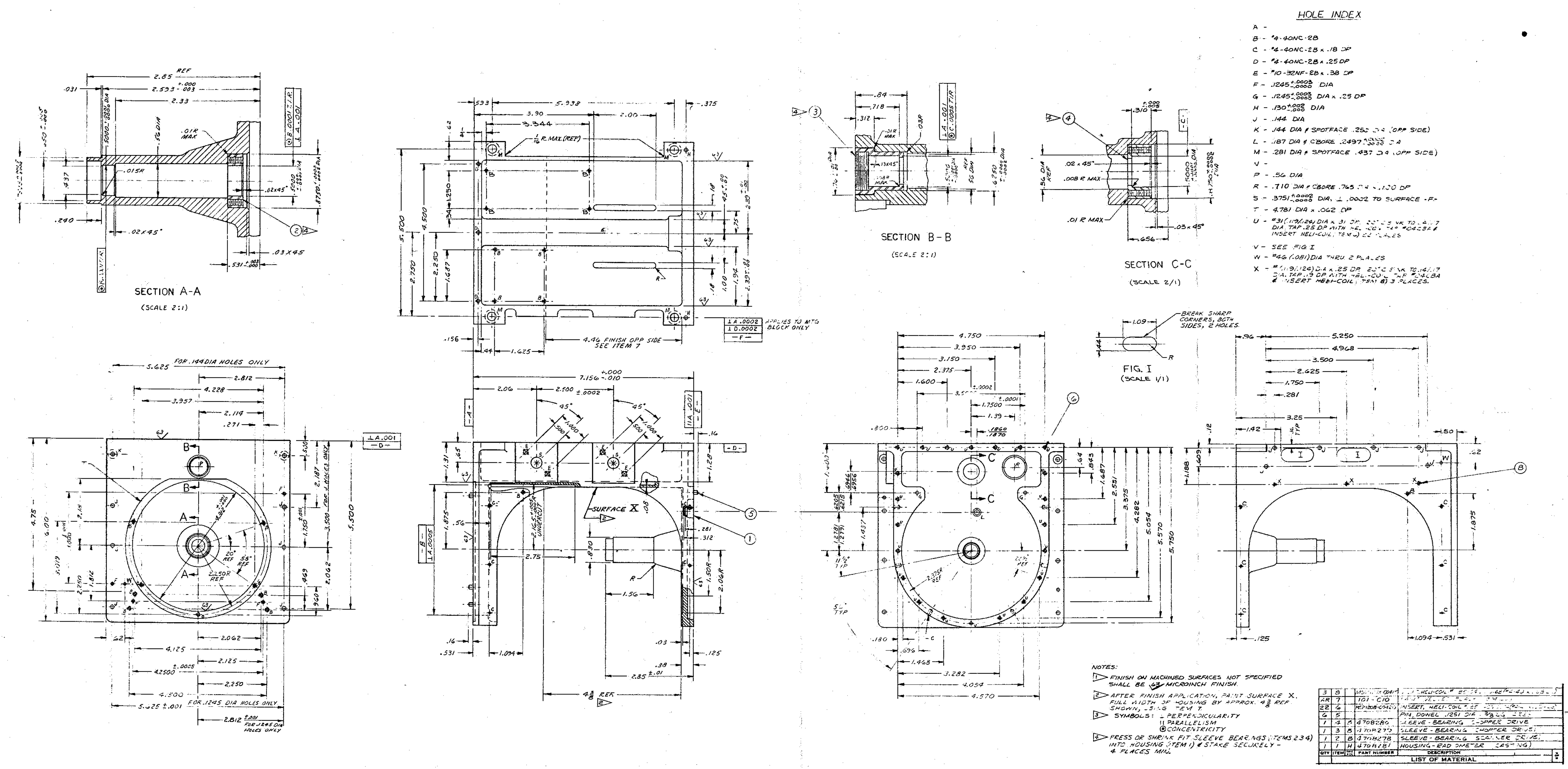

Figure 4 Primary Housing Assembly

FOLDOUT FRAME

6-A

FOLDOUT FRAME

6-B

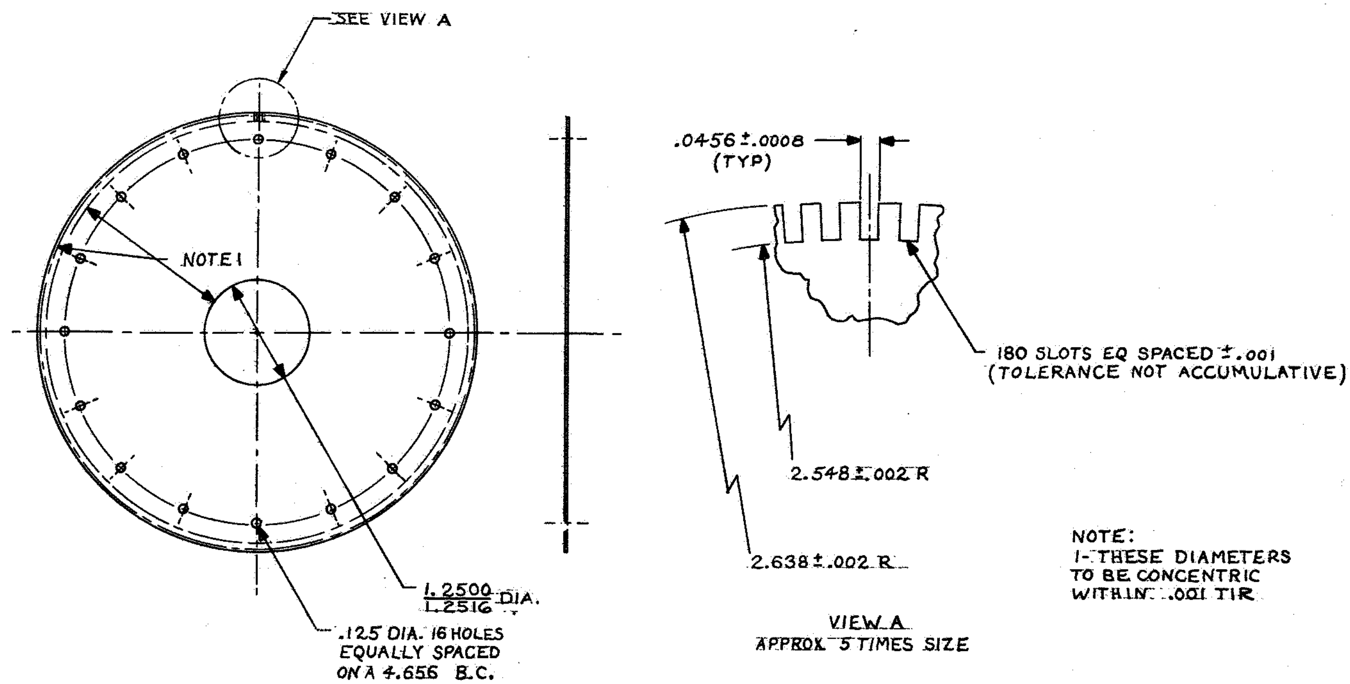

Figure 5 Chopper Disk

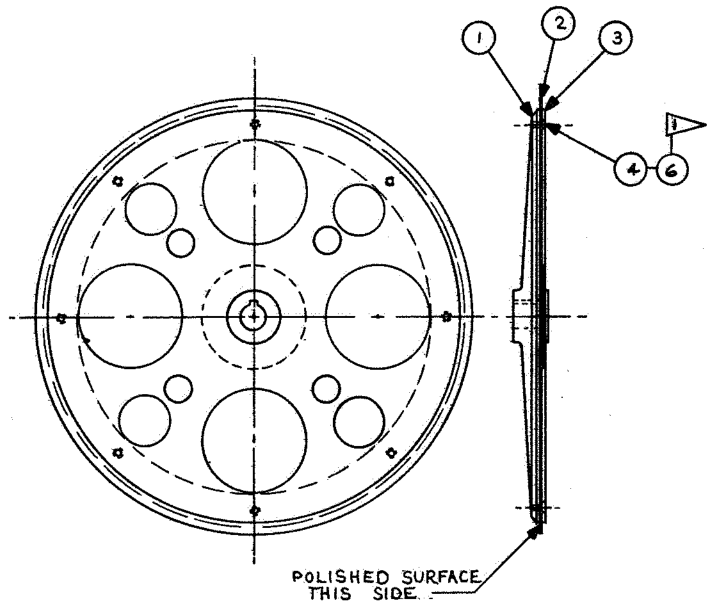

QTY.	ITEM	SIZE	PART NUMBER	DESCRIPTION
AR	6		LOCTITE "D"	LIQUID STAKING COMPOUND
REF	5	A	4708354	ASSEMBLY PROCEDURE & SPEC
8	4		AN505C2R3	SCR, MACH, 82° FH, CRES #2-56 x 3/16
1	3	C	4708348	RING, RETAINING (CHOPPER SUPPORT)
1	2	C	4708347	DISK - CHOPPER
1	1	C	4708349	CHOPPER SUPPORT

LIST OF MATERIAL

Figure 6 Chopper Disk Assembly

3.0 OPTICS

The optics consist of a scanning mirror, primary telescope, and relay lenses. Radiation from the source is reflected off the scanning mirror and focused on the chopper by the primary telescope; it is then transferred to the infrared detector by the relay lenses. The scanning mirror assembly is shown in Figure 7. The mirror is made of 304 stainless steel and polished to a flatness of 1.5 wavelengths of visible light. The primary telescope assembly is shown in Figure 8; it consists of a 4 inch, f/1 paraboloid and a 2.4 inch diameter folding flat. The telescope has a blur circle (90 percent of energy) 1.2×10^{-3} inch in diameter at the primary (chopper) focus.

The design data for the relay optics are given in Table 2, and the mechanical assembly is shown in Figures 9 and 10. The clear apertures listed in the table are those of the axial beam. The first two germanium elements (doublet) in the relay optics (very nearly) collimate the f/1 beam from the 0.25 mm square primary image at the chopper plane. The last two germanium elements, the f/8 focusing and aplanatic lenses refocus the radiation on the 0.5 mm square infrared detector at the secondary focus. The f/1 doublet has a blur circle of 1.5×10^{-3} inch in diameter measured at the primary focus. The f/8 lens has a blur circle of 1×10^{-3} inch and the aplanatic lens a blur circle of 2.5×10^{-3} inch, both measured at the secondary (detector) focus.

The relay optics magnify the 4 inch focal length of the primary telescope by 2X. When combined with the infrared detector of sensitive area 0.553 mm x 0.449 mm, the nominal instantaneous field-of-view is then 2.6 mr x 2.2 mr.

The spectral response is determined by a 10.5 to 12.5 micron interference filter, whose transmission is shown in Figure 11. The peak transmission is 90 percent at 10.8 microns; the transmission is 50 percent of the peak at 10.44 microns and 12.53 microns. Average transmission between the 50 percent of peak wavelengths is 80 percent. Transmission is less than 0.1 percent at 9.86 microns and below and from 13.07 microns to 18.25 microns.

Table 2

Relay Optics Design

Element	Radius	Separation/Thickness	Material	Aperture Radius
		0.6507	Vacuum	
2	-0.827			0.38
		0.311	Ge	
	-0.9199			0.52
		0.2297	Vacuum	
3	-6.235			0.61
		0.300	Ge	
	-3.646			0.64
		6.000	Vacuum	
4	30.03			0.65
		0.300	Ge	
	∞			0.64
		7.911	Vacuum	
7	0.2519685			0.14
		0.1259842	Ge	
	0.1889764			0.08
		0.189	Vacuum	

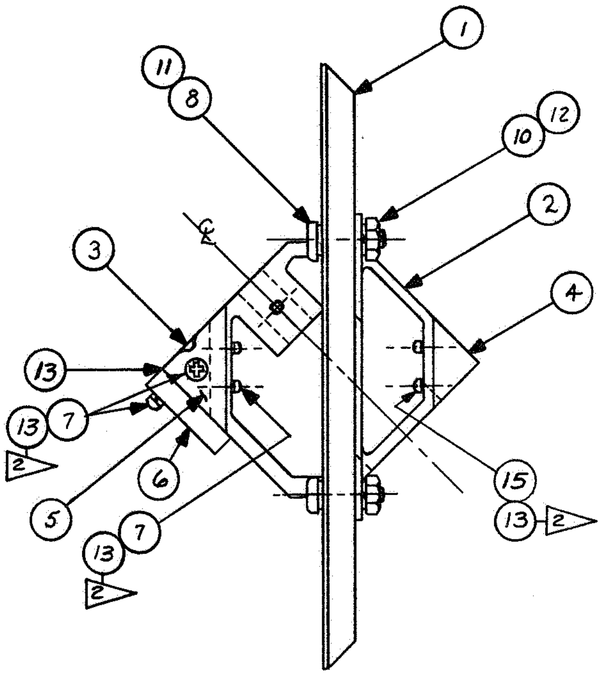

NOTES:

1. ASSEMBLY TO BE DYNAMICALLY BALANCED TO WITHIN 50 MICRO-INCHES.
2. REMOVE EXCESS LOCTITE (IT. 13) BEFORE INSTALLING SCREWS.

QTY.	ITEM	DWG SIZE	PART NUMBER	DESCRIPTION
2	15		MS51957-3	SCR, MACH, PAN HD, CRES (#2-56 x 1/4)
REF	14	A	4708315	ASSEMBLY PROCEDURE & SPECIFICATIONS
AR	13		LOCTITE "D"	LIQUID STAKING COMPOUND
4	12		MS35649-64	NUT, PLAIN, HEX, CRES (#6-32)
4	11		MS15795-805	WASHER, FLAT, CRES (#6)
4	10		MS35338-79	WASHER, LOCK, SPLIT, CRES (#6)
	9			
4	8		MS51957-31	SCR, MACH, PAN HD, CRES (#6-32 x 5/8)
5	7		MS51957-4	SCR, MACH, PAN HD, CRES (#2-56 x 5/16)
1	6	B	4708314	COUNTERWEIGHT END
2	5	B	4708313	COUNTERWEIGHT SIDE
1	4	B	4708312	COUNTERWEIGHT
1	3	B	4708311	COUNTERWEIGHT
1	2	D	4708310	SUPPORT FRAME, MIRROR
1	1	C	4708309	MIRROR, ROTATING

LIST OF MATERIAL

Figure 7 Scanning Mirror Assembly

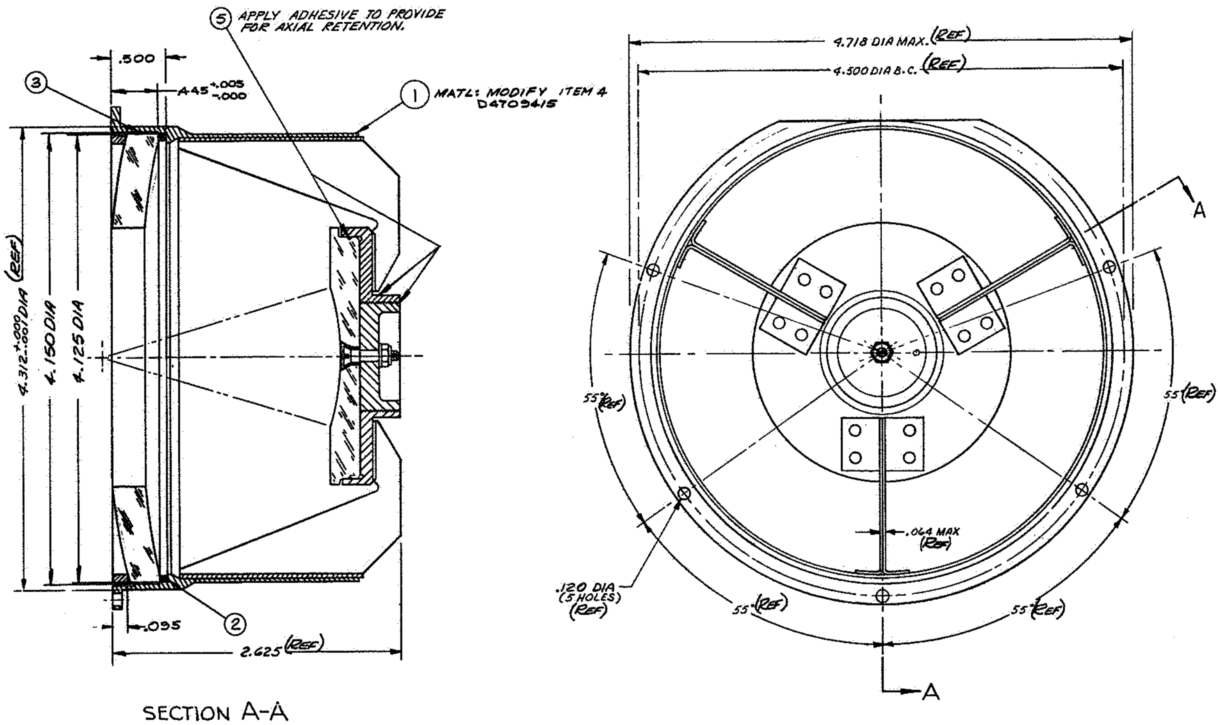

QTY.	ITEM	[illegible]	PART NUMBER	DESCRIPTION
AR	5		RTV 108	SILICONE ADHESIVE/SEALANT. (G.E.)
1	4	D	4709415	TELESCOPE ASSEMBLY
1	3	B	4708331	GASKET, TEFLON
1	2	B	4708330	BUMPER SPACER, NYLON
1	1	D	THIS DWG-1	TELESCOPE ASSEMBLY, MODIFIED

LIST OF MATERIAL

Figure 8 Primary Telescope Assembly

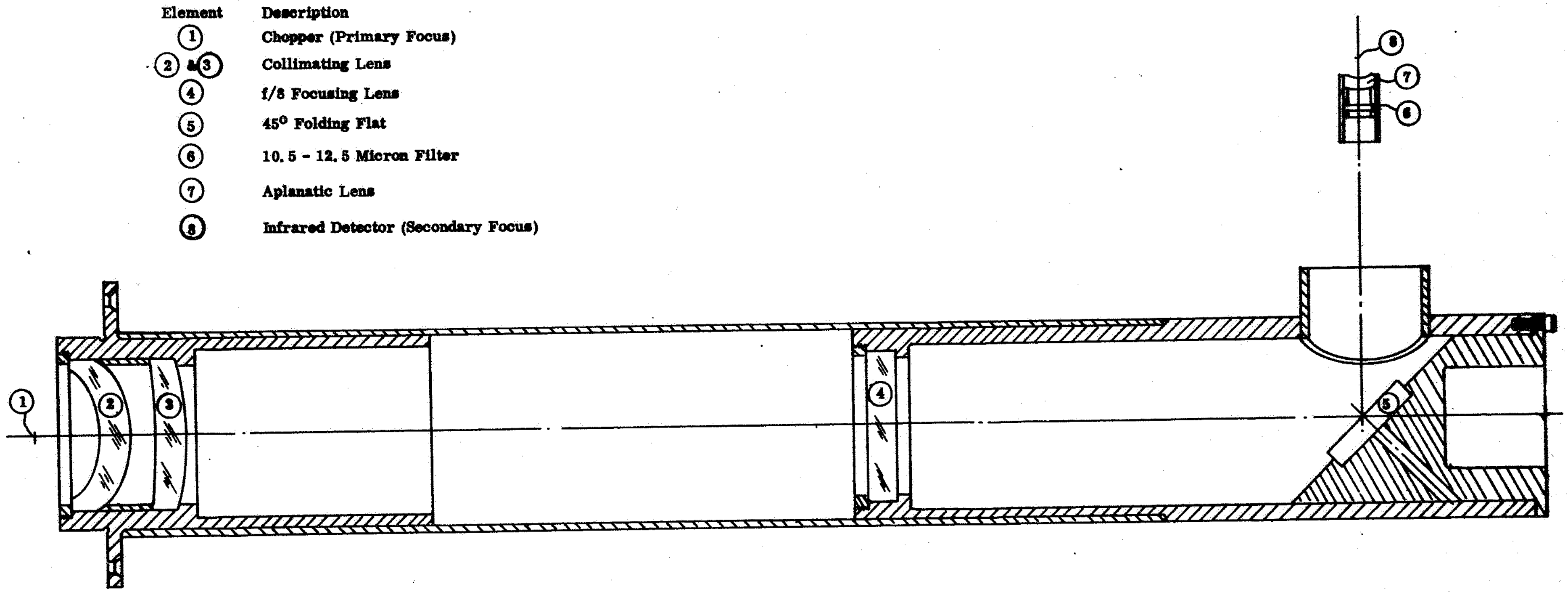

Figure 9 Relay Optics Assembly

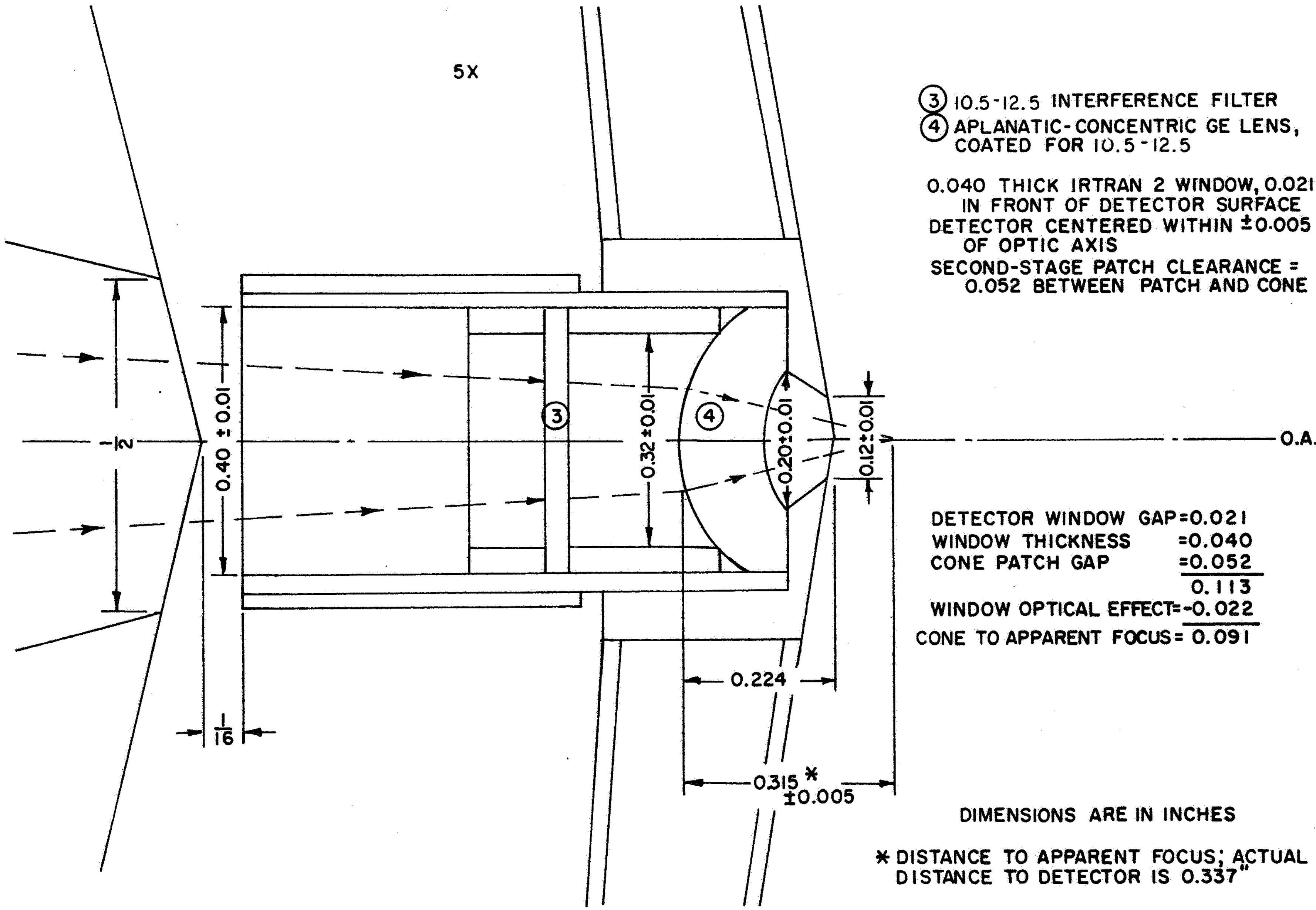

Figure 10 Optics Mounted in First-Stage Patch

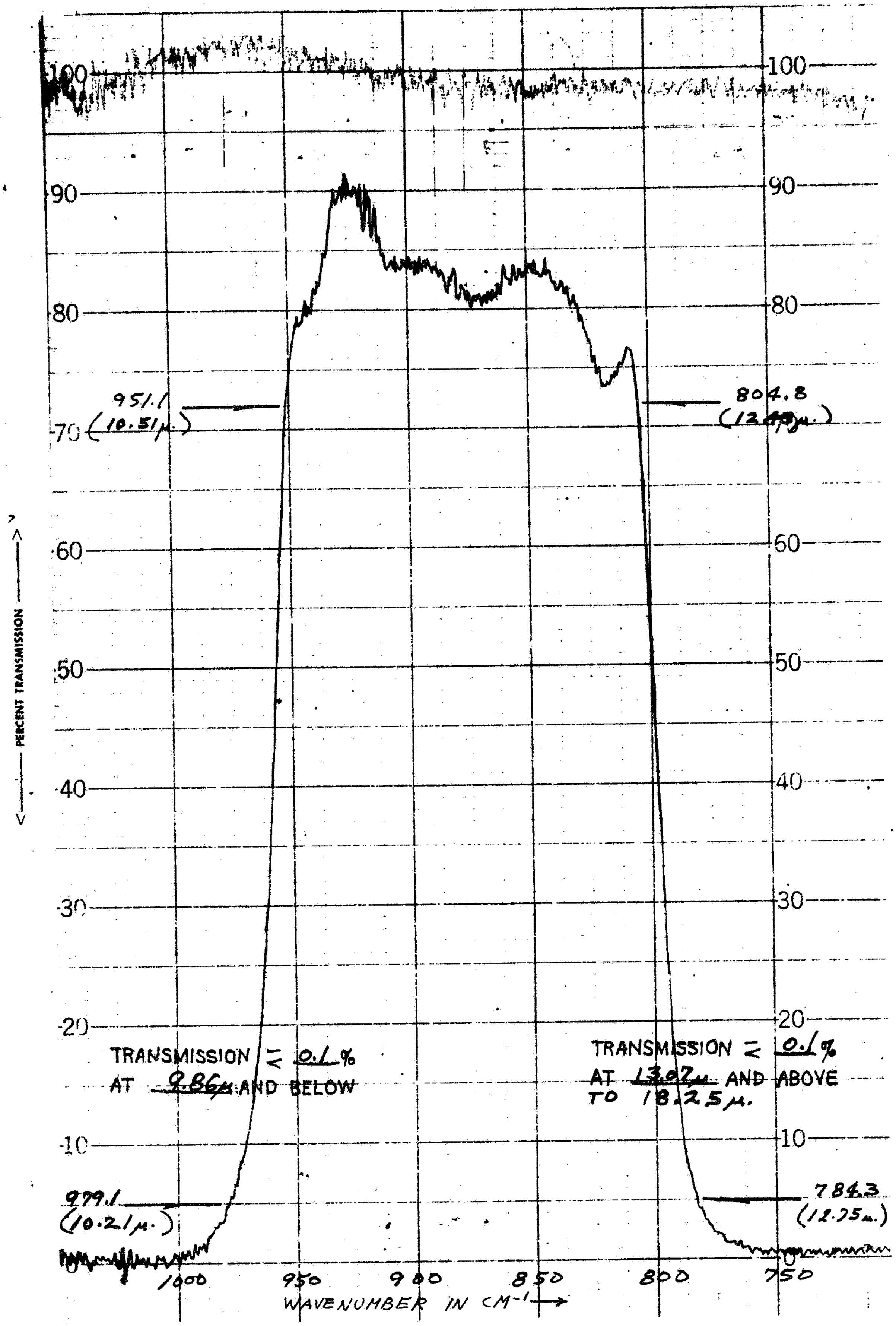

Figure 11 Spectral Transmittance of Interference Filter

4.0 INFRARED DETECTOR

The infrared detector for the day-night radiometer may be a $Cd_x Hg_{1-x} Te$ photovoltaic detector (C. Verié and J. Ayas, Appl. Phys. Lett. 10, 241, 1 May 1967) or a DLK21 photoconductive detector (Honeywell Radiation Center, Boston, Mass.). Both detectors operate at or near liquid nitrogen temperature (77 degrees K). The usual characteristics of a photovoltaic detector with a maximum response between 10.5 and 12.5 microns and an area less than 1 square millimeter are given in Table 3 (private communication from C. Verié). The best detectors have a D* close to 1×10^{10} cm $hz^{1/2}$ /watt, a value that is presently not reproducible.

Table 3

Typical Characteristics of Photovoltaic Detector

D* (peak spectral, 900, 1):	5×10^9 cm $hz^{1/2}$ /watt
Area	less than 1 mm^2
Spectral peak	10.5 to 12.5 microns
Dark dynamic resistance	50 ohms
Operating temperature	77^o K
Response time	less than 10 nsec

The typical characteristics of a DLK 21 photoconductive detector are given in Table 4 together with those of the detector used in the day-night radiometer. The spectral response of the radiometer detector is shown in Figure 12.

Table 4

Characteristics of Photoconductive Detector

	Typical	Day-Night Radiometer
D* (500^oK, 1000, 1)	2×10^9 min	3.82×10^9
Area	0.5 mm x 0.5 mm	0.533 mm x 0.444 mm
Spectral Peak	10-13 microns	11.5 microns
Resistance	10 ohms min	171 ohms
Operating temperature	77^oK	77^oK
Optimum bias current	-	0.9 ma

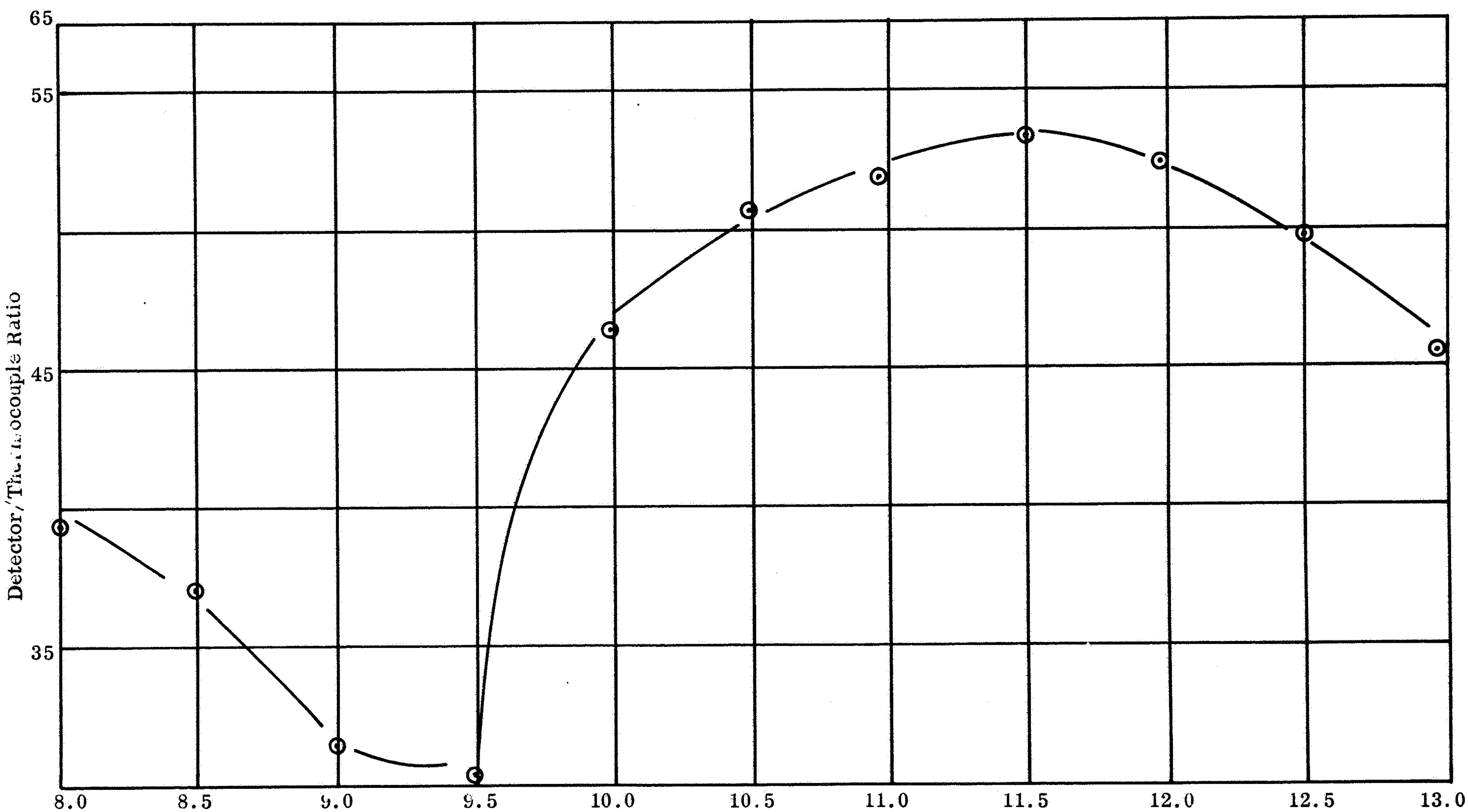

Figure 12 Detector Spectral Response

Experimental $Cd_x Hg_{1-x} Te$ detectors have been made by Santa Barbara Research Center, Goleta, California. These detectors have a resistance of 30 to 300 ohms per square, a response time of 1 to 100 nsec, and a spectral peak of 9 to 13 microns.

There is no joule heating in the photovoltaic detector to increase the thermal load on the second-stage patch. Moreover, the joule heating of the photoconductive detector at optimum bias produces a temperature rise of only 0.7 degree K in a patch at 77 degrees K (Part I, Section 2.1.6.3).

The second-stage patch was initially designed to hold a detector package similar to that presently used for the PbSe element in Nimbus High Resolution Infrared Radiometer (Contract NAS5-668). This requires the use of an overcoat or encapsulating material to protect the sensing element from atmospheric effects. At present, however, no such coating is known for the DLK 21, although an investigation is underway at Honeywell Radiation Center. The sensing element is therefore enclosed in a space filled with dry inert gas and radiation admitted through a clear Irtran II (Eastman Kodak) window. This change, plus the desire of Honeywell to use an assembly similar to ones already in use, resulted in a detector package which extends beyond the height (0.32 inch) of the rest of the second-stage patch.

The detector package is shown in Figure 13. The housing is made of Kovar to match the thermal expansion of the glass beads used to hermetically seal the electrical feed-throughs. This entire assembly containing a detector element was originally mounted in a dewar for laboratory testing.

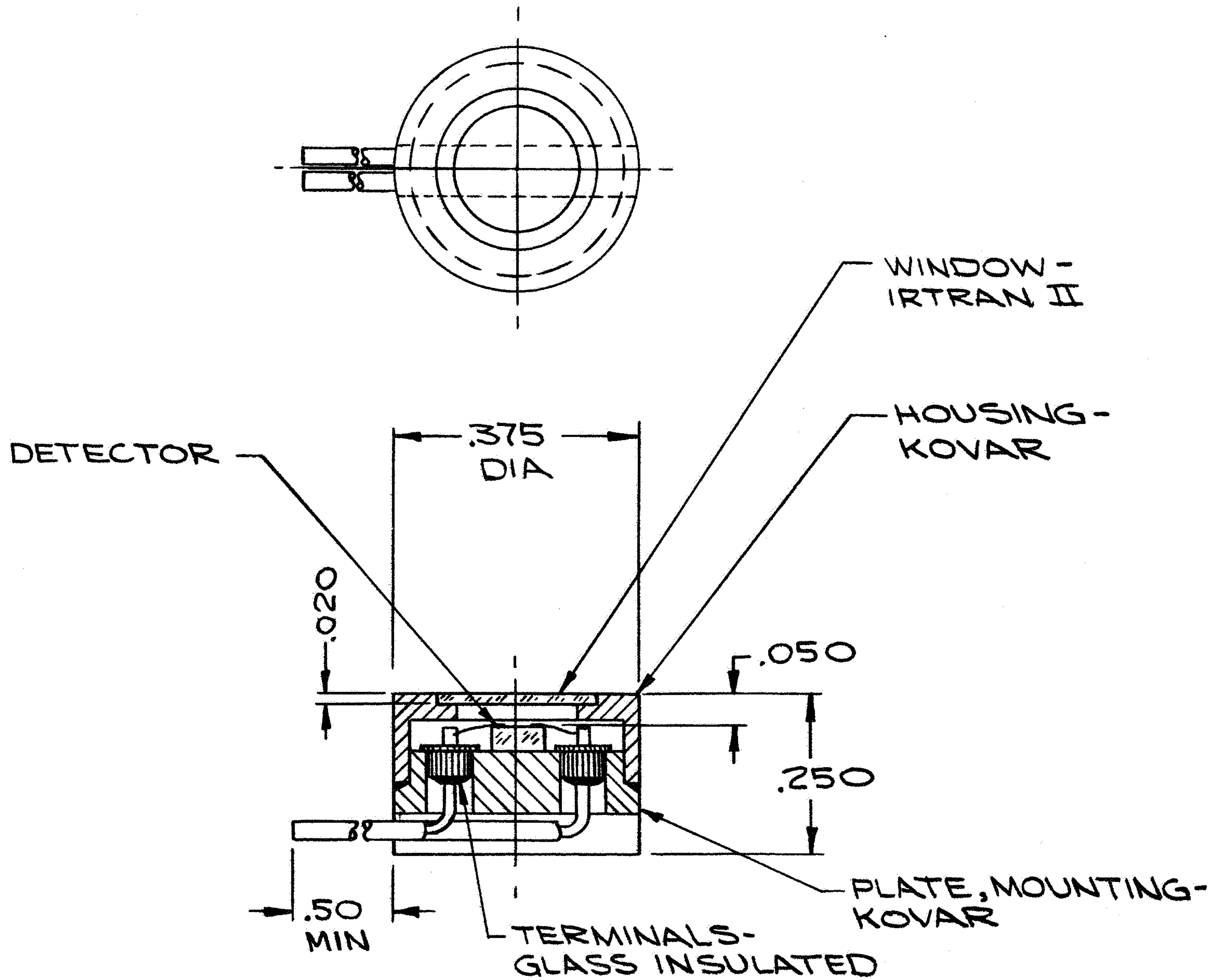

Figure 13 Detector Assembly

5.0 ELECTRONICS

Figure 14 is a block diagram of the radiometer electronics. The infrared cell at the secondary image plane detects the signal modulated by a mechanical chopper at the primary image plane. The detector signal is amplified by the preamplifier and video amplifier. It is then synchronously demodulated by the reference signal, filtered, and combined with the correction voltage. The input to the reference signal generator is a chopper modulated light beam, which is detected by the photodiode. The correction voltage is generated during the time the radiometer is viewing cold space. This interval is indicated by the space scan gate generator, which is operated by the magnetic pickup in the gear train to the scan mirror.

The signal from the infrared detector is fed to a transistor preamplifier manufactured by Perry Associates, Brookline, Mass. The specifications for the preamplifier are given in Table 5 and the broadband noise performance in Figure 15. The device is specifically designed to match the low impedance of the infrared detector (50 to 200 ohms) while preserving low noise performance without the aid of an input transformer or other inductive component.

Table 5

Preamplifier Specifications
(Perry Model 600)

Gain (Rg = 50)	40 db
Bandwidth (Rg = 100)	20 hz to 100 khz
Band Flatness	1 db
Noise Figure (Broadband, Rg = 100)	2 db
Input Impedance	50 ohms
Output Impedance (F = 1 khz)	500 ohms
Output Level Maximum	1 volt rms
Operating Temperature	-55° to $+125^{\circ}$C
Power Requirements	± 12 volts 6 ma
Mechanical Size	2" x 2" x 1"

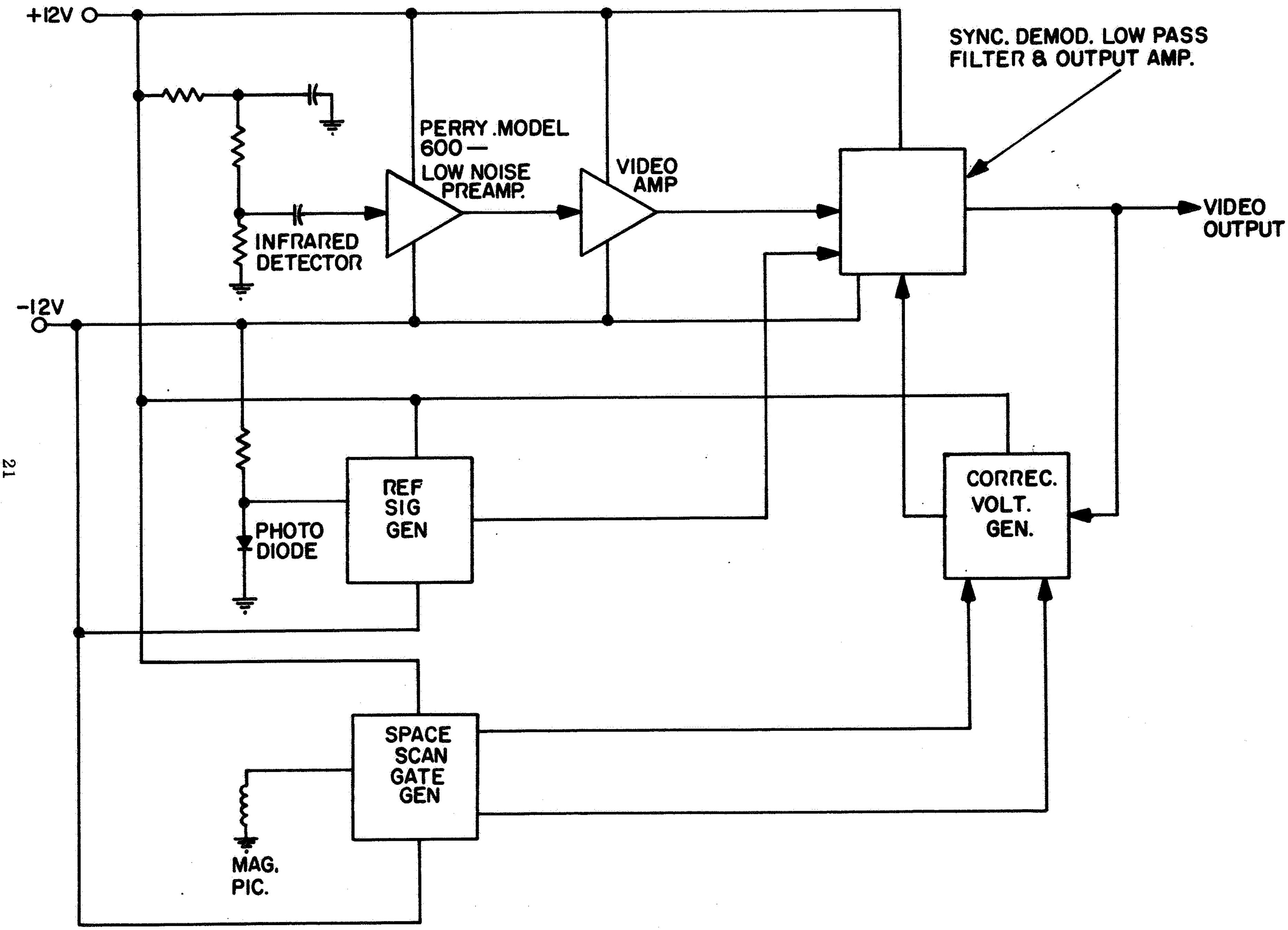

Figure 14 Electronics Block Diagram

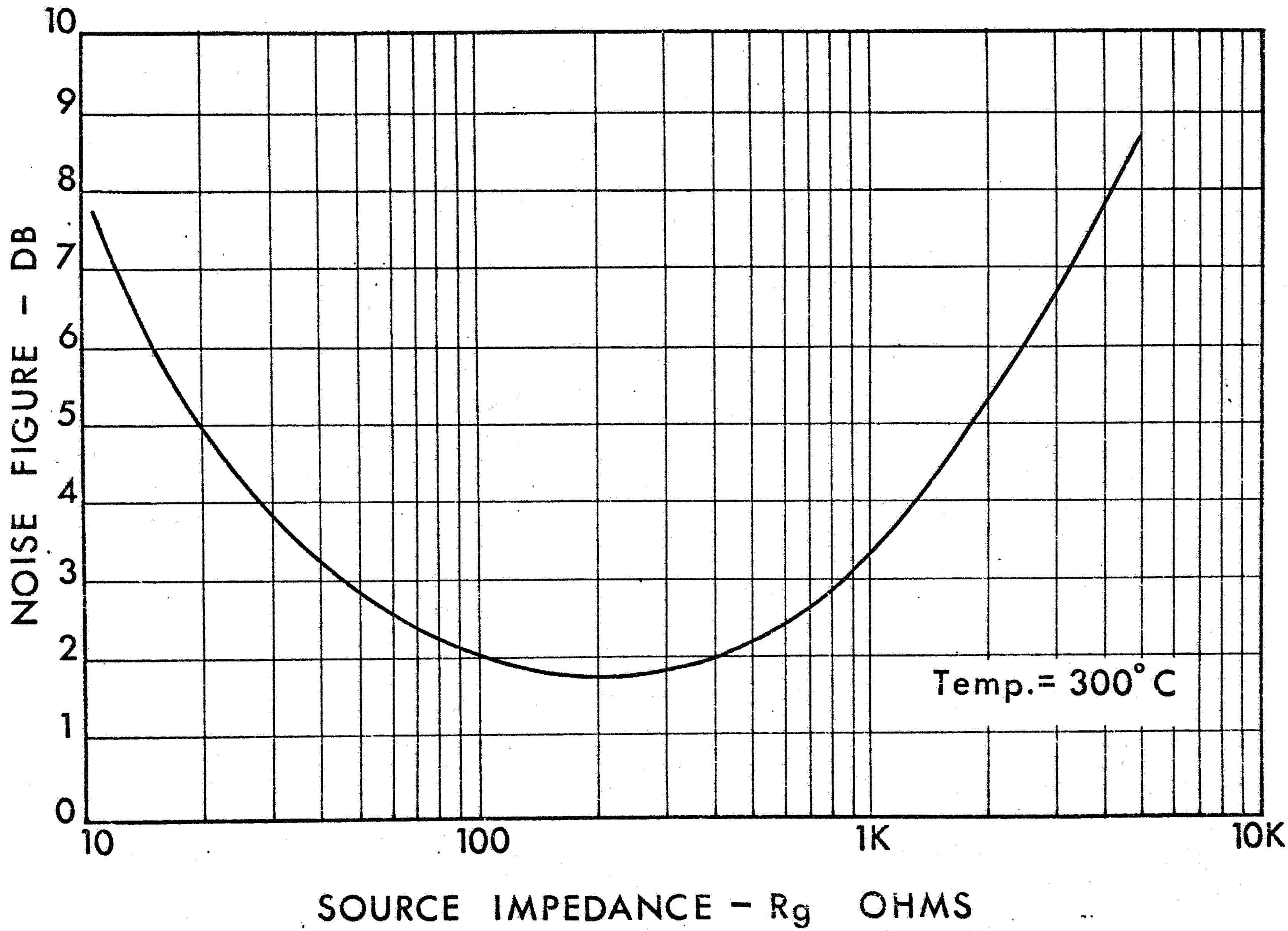

Figure 15 Preamplifier Broadband Noise Performance

Schematics of the five remaining blocks are given in Figures 16 through 20. Most circuits utilize a microcircuit monolithic amplifier, the μA709. This circuit component can be used for a-c or d-c amplification, as a comparator, and as a multivibrator.

The video amplifier (Figure 16) serves as an amplifier and as a driver for the demodulator. The maximum amplifier gain is about 60 db with a variation of 6 db. The low frequency cutoff is about 700 hz, and the high frequency cutoff is 47 khz at maximum gain and 70 khz at minimum gain.

The demodulator (Figure 17) synchronously rectifies the video amplifier output. The switching voltage from the reference signal generator (Figure 18) is fed in at LB039. The rectified output is applied at the common source connection of the CM602's.

The low-pass filter response in combination with the demodulator is shown in Figure 21. The filter causes a delay that is constant (184 microseconds) for all frequencies over the passband.

The output amplifier provides amplification of the demodulated and filtered signal from d-c to beyond the passband. It also serves as a mixing point for the video and chopper correction inputs.

The reference signal generator (Figure 18) processes the 6 khz signal from the chopper photodiode to a 6 khz square wave for demodulation of the video signal. The first amplifier is an a-c amplifier with a voltage gain variation of 5.6 db. The second is a saturating amplifier which squares up the video signal until now, a sinusoidal signal. The output is a 6 khz square wave approximately 22 volts peak to peak.

The correction voltage generators (Figure 19) provides output correction for the difference in signal between the chopper and space. The gate formed by the upper CM602 and associated components passes the video output to the comparator (first μA709) during the time the mirror is scanning space (about one-tenth of a scan period). During the remainder of the scan, the lower CM602 gates the comparator input to ground.

If the output video (E_O) is positive with respect to the reference, the comparator has a negative going output and the opposite is true for a negative going video. If the comparator input is equal to the reference level, the comparator output is zero. This pulsed output with a one-tenth duty cycle is integrated by the components connecting the pair of μA709's. The integrated d-c level is amplified by the non-inverting amplifier formed by the second μA709, which provides the correcting input, E_C, to the output amplifier.

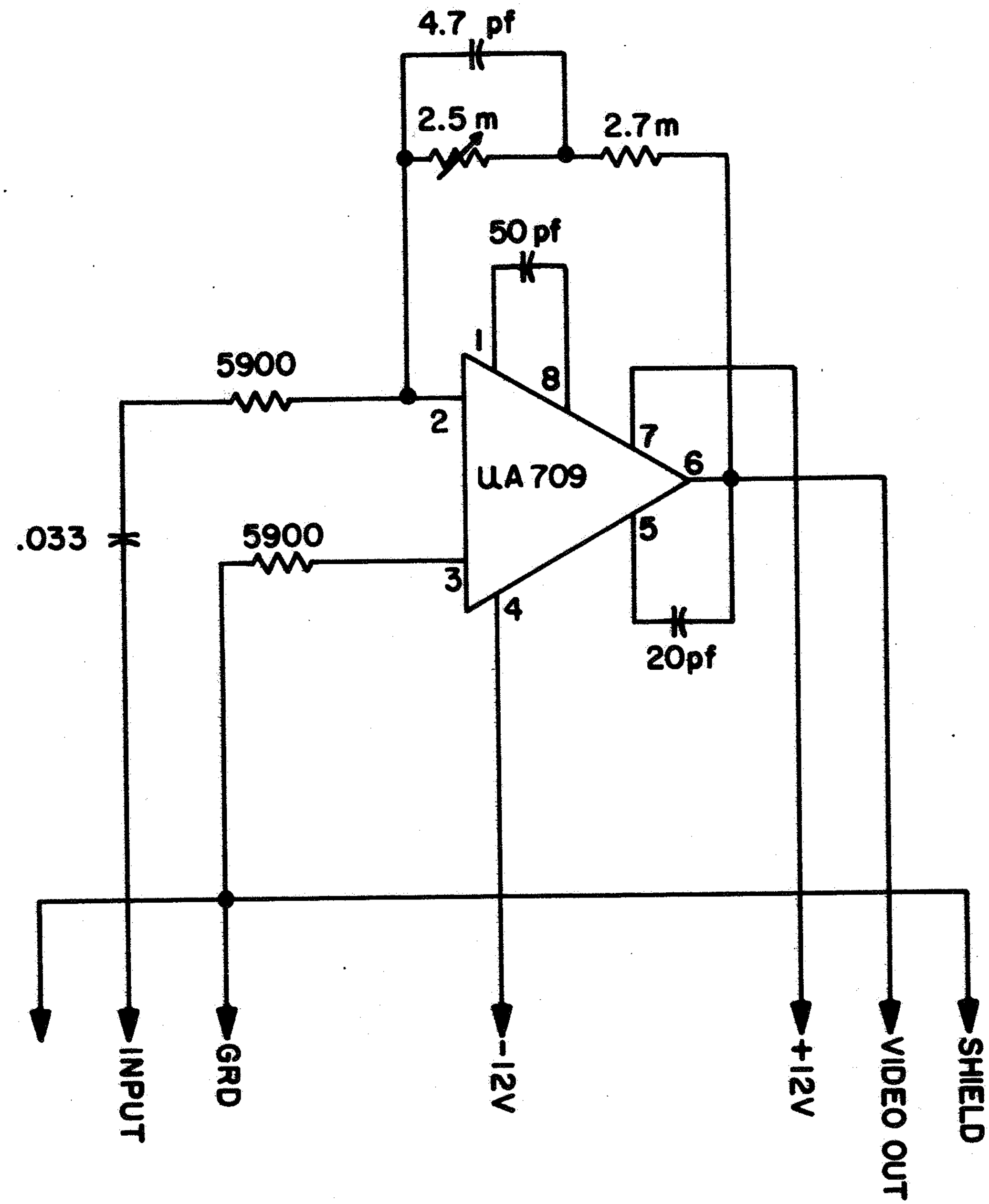

Figure 16 Video Amplifier

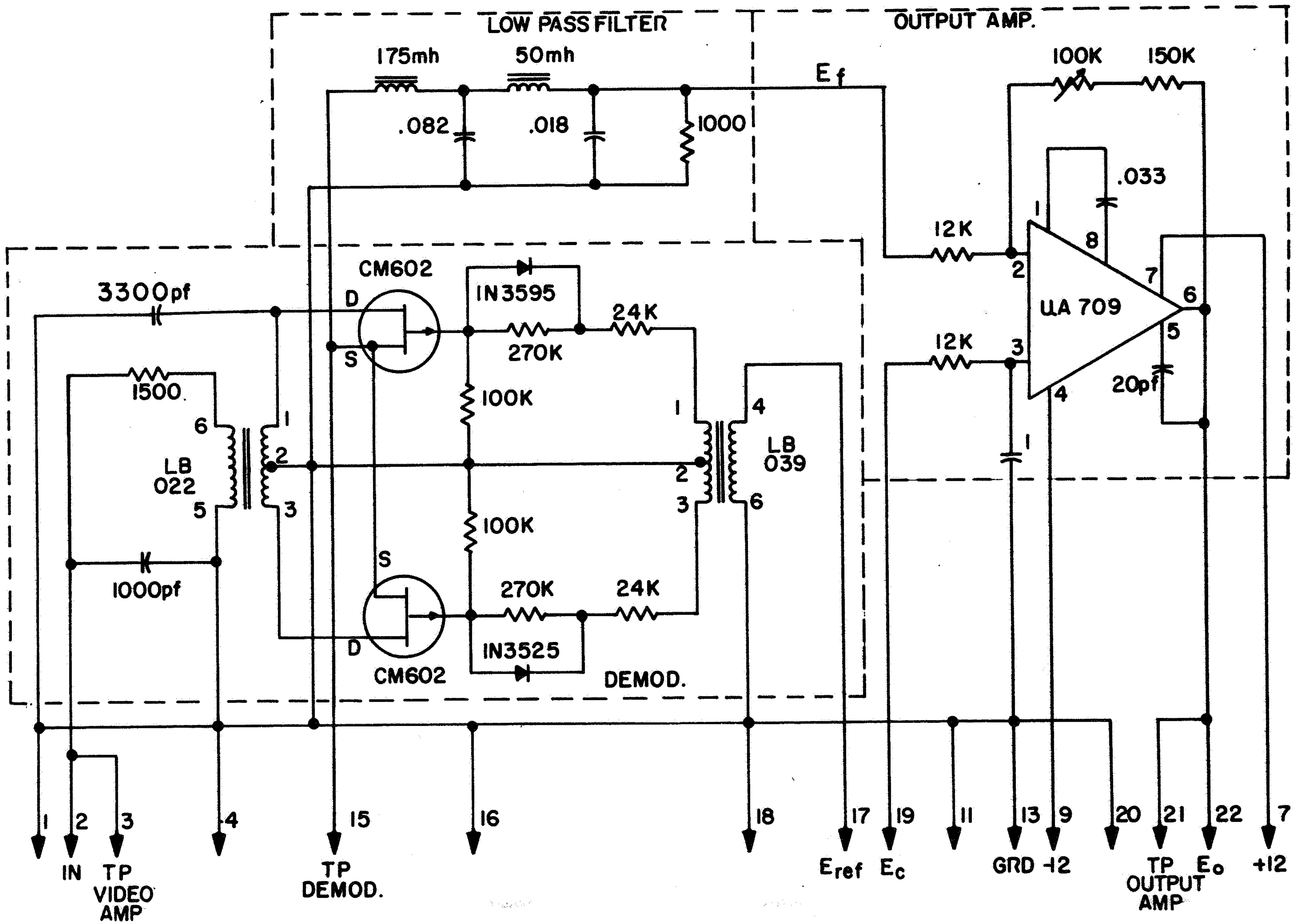

Figure 17 Demodulator, Low-Pass Filter, and Output Amplifier (Board No. 1)

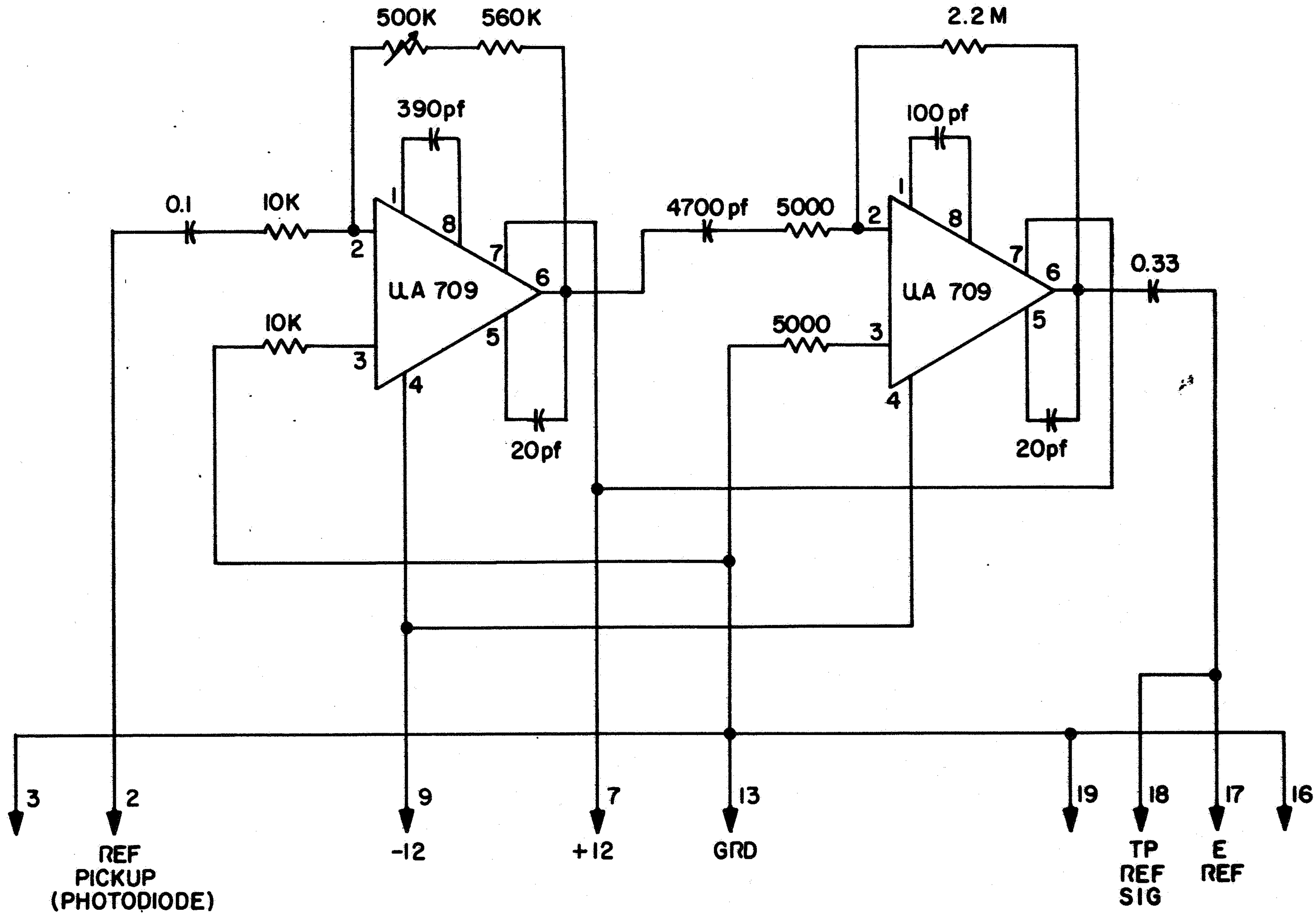

Figure 18 Reference Signal Generator (Board No. 2)

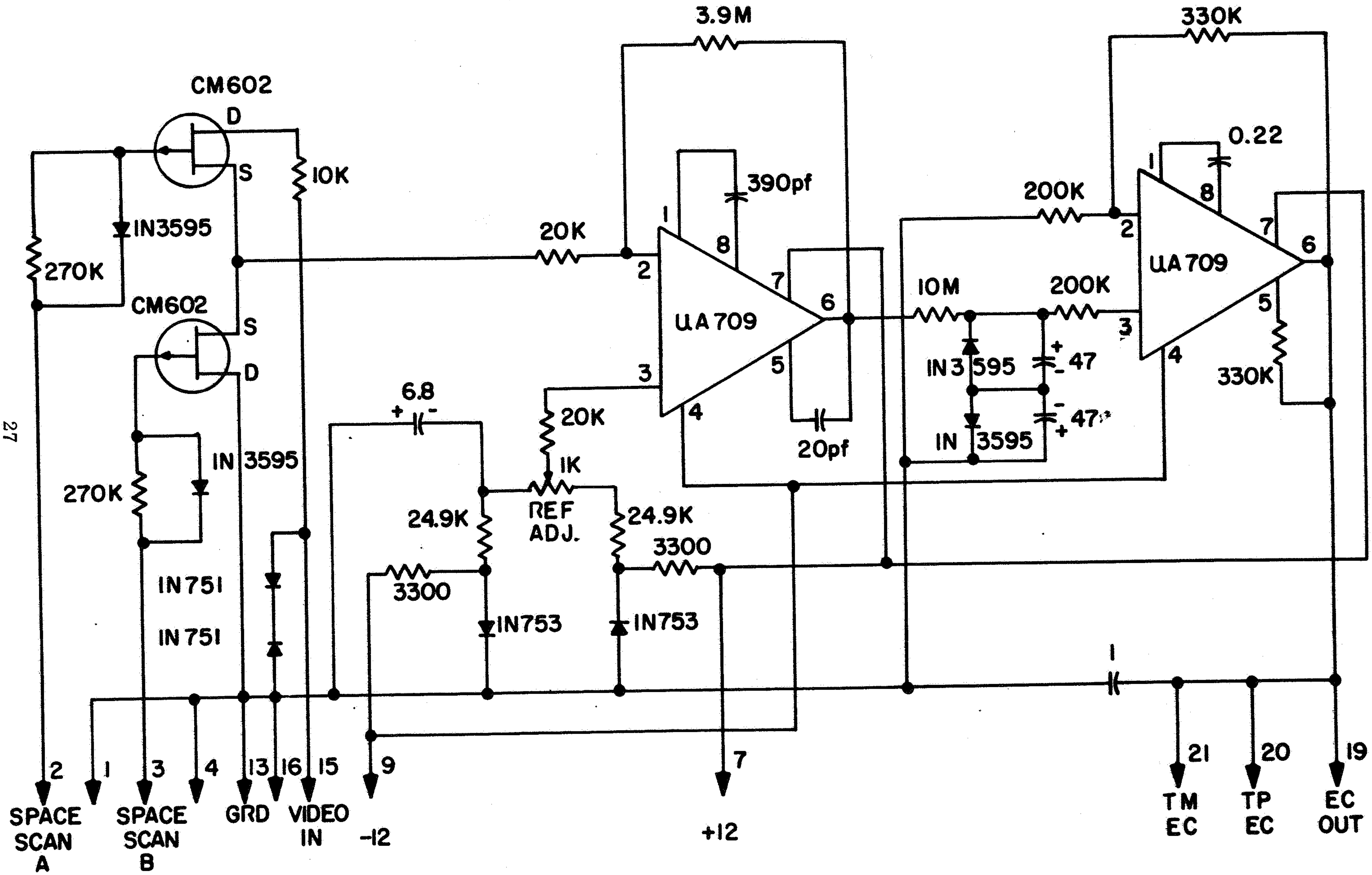

Figure 19 Correction Voltage Generator (Board No. 3)

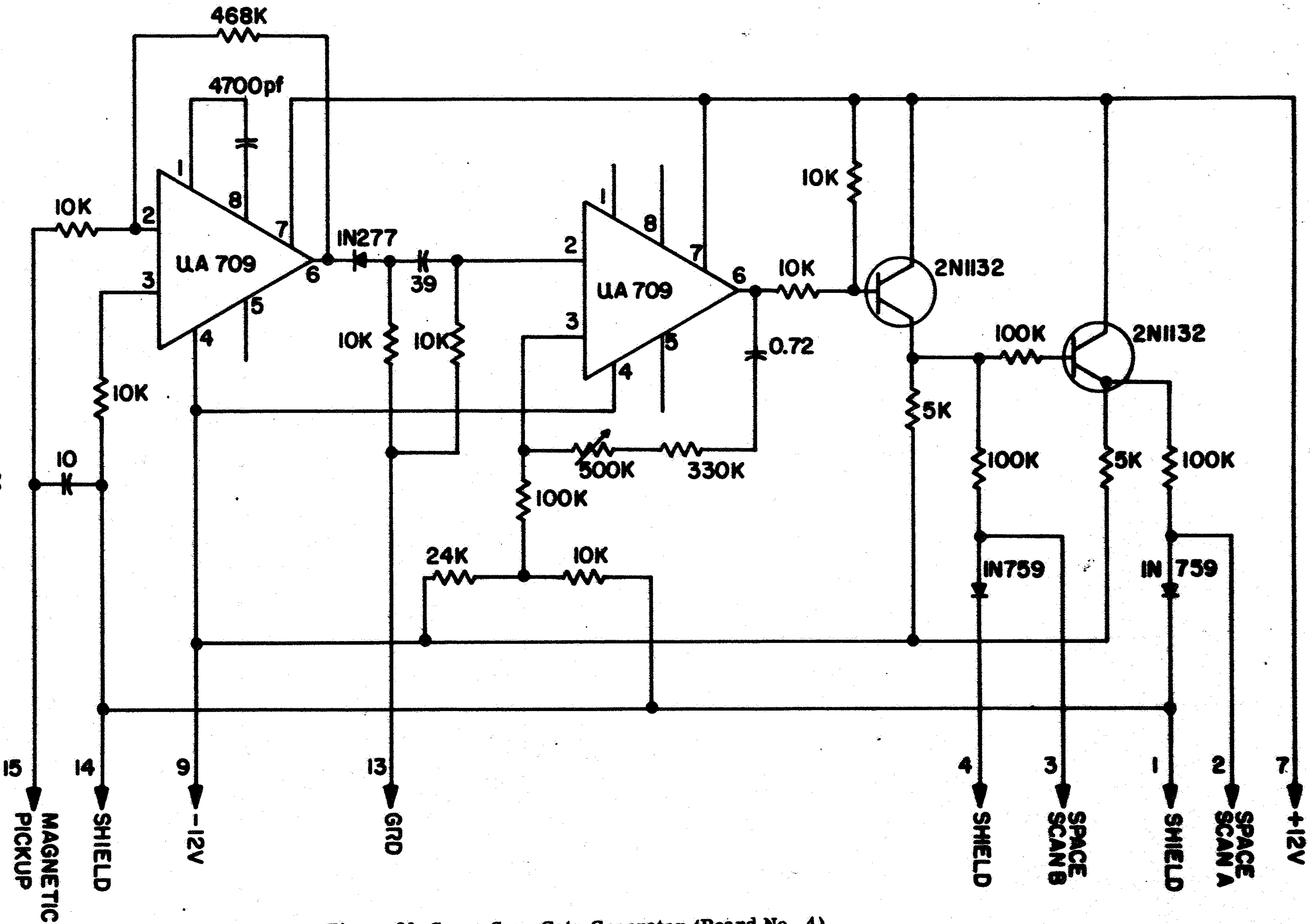

Figure 20 Space Scan Gate Generator (Board No. 4)

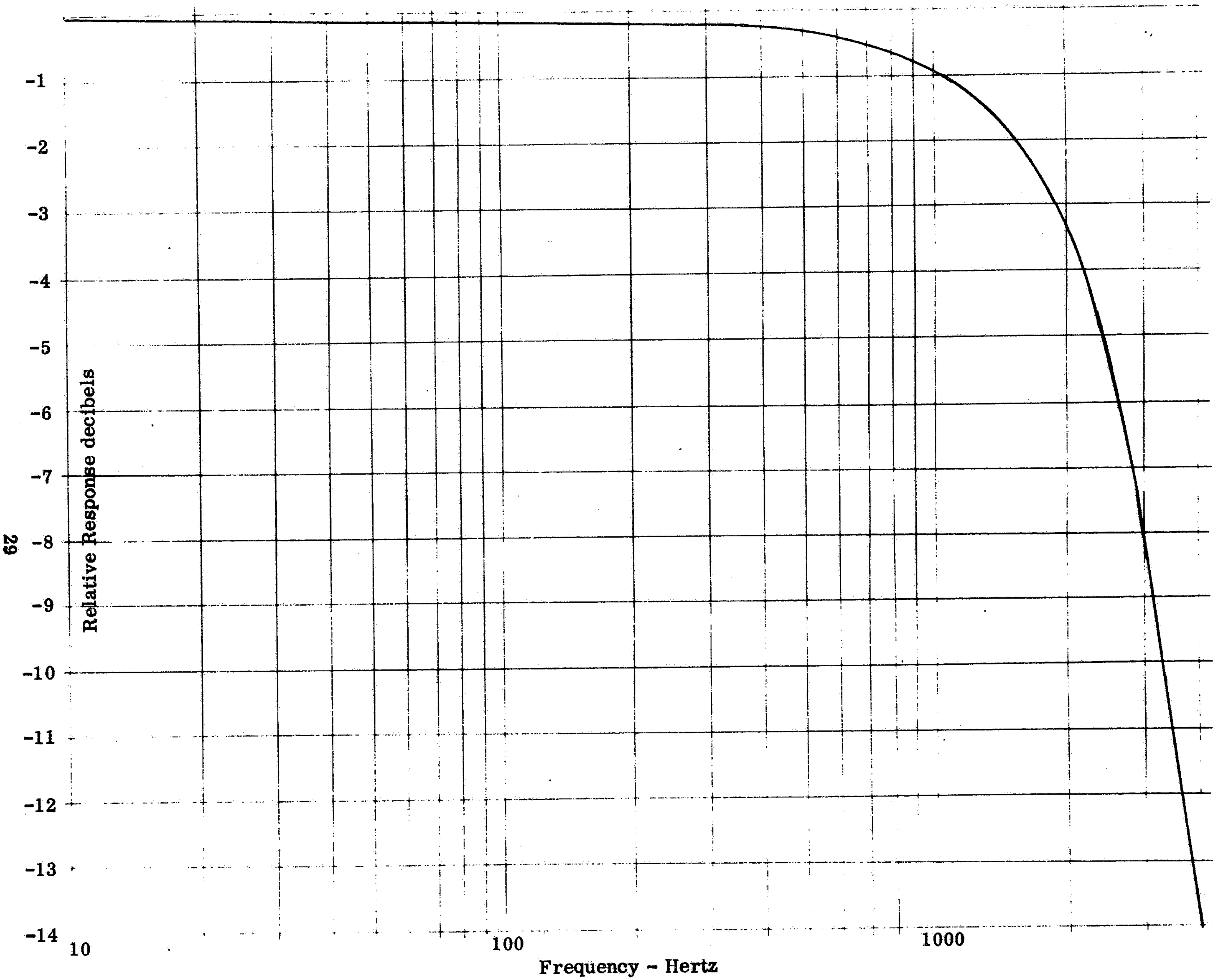

Figure 21 Demodulator and Low Pass Filter Response

The correction voltage generator has a gain characteristic such that

$$E_o = mE_c + V_{th}$$

where E_o is the input voltage level. If the reference level is perfectly adjusted, V_{th} is zero. In measurements taken in the laboratory, m had a value of 1/26.8 and V_{th} a value of +0.025 volt.

Referring again to Figures 17 and 19, it can be seen that the significant part of the above loop with respect to the chopper error is the output amplifier and the correction voltage generator. The following definitions are made:

E_f = the demodulated and filtered video signal input to the output amplifier

E_c = the chopper correction d-c input to the output amplifier

E_o = the video output and the input to the correction voltage generator

E_{ch} = that portion of the demodulated video signal caused by the chopper

E_{tar} = that portion of the demodulated video signal caused by the target

We then have $E_f = E_{ch} - E_{tar}$, $E_o = K_1 E_F + K_2 E_c$, and $E_c = K_3 (E_o + vth)$. Then $E_o = K_1 (E_{ch} - E_{tar}) + K_2 E_c$. If $E_{tar} = 0$, (which is the case when looking at space), then $E_o (E_{tar} = 0) = K_1 E_{ch} + K_2 E_c$. Therefore $E_c = K_3 (K_1 E_{ch} + K_2 \cdot E_c + vth)$ or $E_c = K_1 K_3 E_{ch}/(1 - K_2 K_3) + K_3 vth/(1 - K_2 K_3)$. This is the correction signal caused by a look at space. Working this back into the original equation $E_o = K1 E_{ch} - K_1 E_{tar} + K_2 E_c$, we have

$$E_o = K_1 E_{ch} - K_1 E_{tar} + \frac{K_1 K_2 K_3 E_{ch}}{(1 - K_2 K_3)} + \frac{K_2 K_3 v_{th}}{(1 - K_2 K_3)}$$

$$E_o = \frac{K_1 E_{ch}}{(1 - K_2 K_3)} - K_1 E_{tar} + \frac{K_2 K_3 v_{th}}{1 - K_2 K_3}$$

From laboratory measurements, $K_1 = -12.8$, $K_2 = 13.7$, $K_3 = 26.8$, $v_{th} = +0.025$; so that

$$E_o \cong 0.035 E_{ch} + 12.8 E_{tar} + v_{th}$$

For a maximum output of 6 volts, $E_{tar} = 0.47$ volt for a 330 degree K target. Considering the chopper to have a maximum effective temperature of 300 degrees K, the chopper signal input to the output amplifier is 0.329 volt. With $E_{tar} = 0$, $E_o = 0.0115 + 0.025$ and the maximum error at the output due to the chopper correction is 11.5 millivolts.

6.0 TEST EQUIPMENT

The test equipment for this program is patterned after the Nimbus bench checkout unit (Contract NAS5-668) with special emphasis on low temperature measurement and recording. Full advantage of existing designs and techniques has been taken.

The test equipment has been divided into two categories, that for the second phase (cooler testing) and that for the third phase (radiometer testing). Figure 22 is a block diagram of the test equipment required for both phases of the program. The test equipment for the radiant cooler is described in Section 3.0, Part I.

A photograph of the electronic test equipment is shown in Figure 23. The cabinets contain the instruments listed in Table 6.

Table 6

Electronic Test Equipment

Cabinet 1	Cabinet 2	Cabinet 3
Honeywell Electronik Multichannel Recorder	Patch Panel	Secondary Voltage Standard
Low Temperature Monitor Unit	Breadboard Electronics (Partial*)	Digital Voltmeter
Calibration Target Temperature Control		Oscilloscope
		Digital Printer
Variacs for Motor Power and Target Heater		Honeywell 1508 Visicorder
Primary 24 vdc Power Supply		Galvanometer Amplifiers (6)

* Remainder is in space chamber

An extended aluminum shroud was constructed to provide a cold space look for the breadboard radiometer. The portion facing the scanner (rather than the copper structure) was painted with 3M Black Velvet. The outer surface of the aluminum is covered with aluminized mylar to offset the thermal loading or the black area and thus maintain the aluminum at a temperature of 100 to 150 degrees K. Figure 24 shows the shroud and the calibration blackbody target mounted in the space chamber.

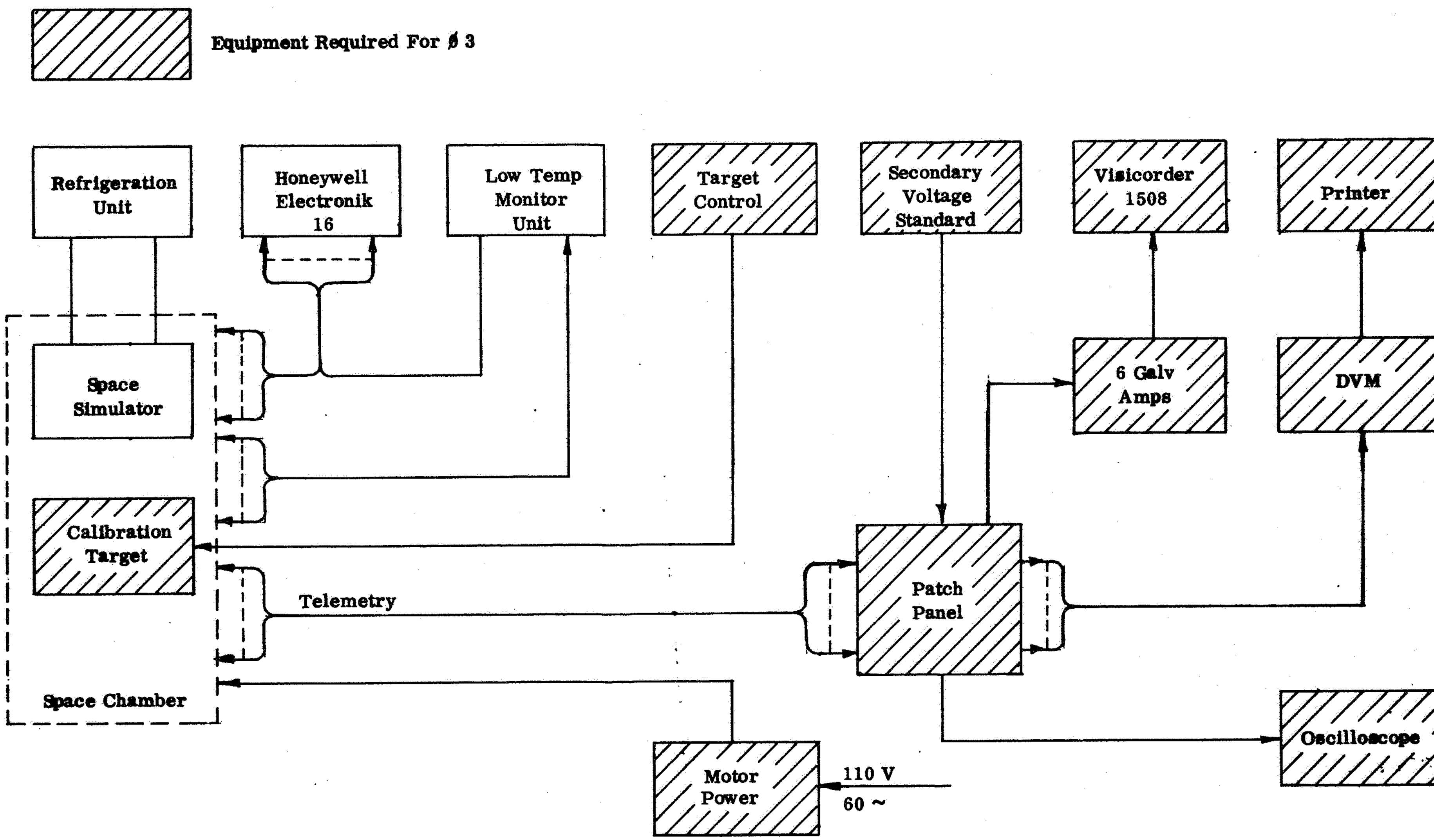

Figure 22 Test Equipment Block Diagram

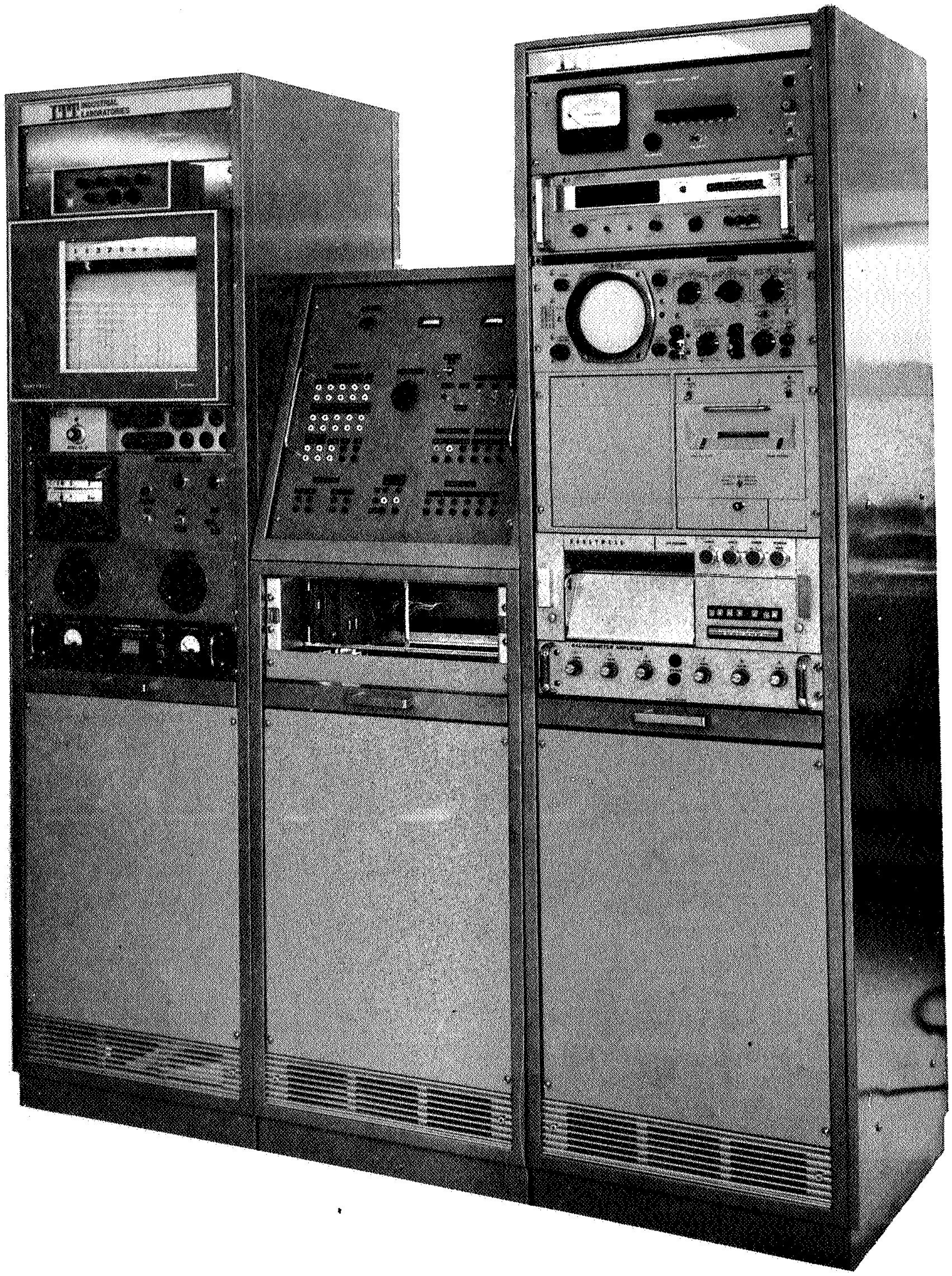

Figure 23 Electronic Test Equipment

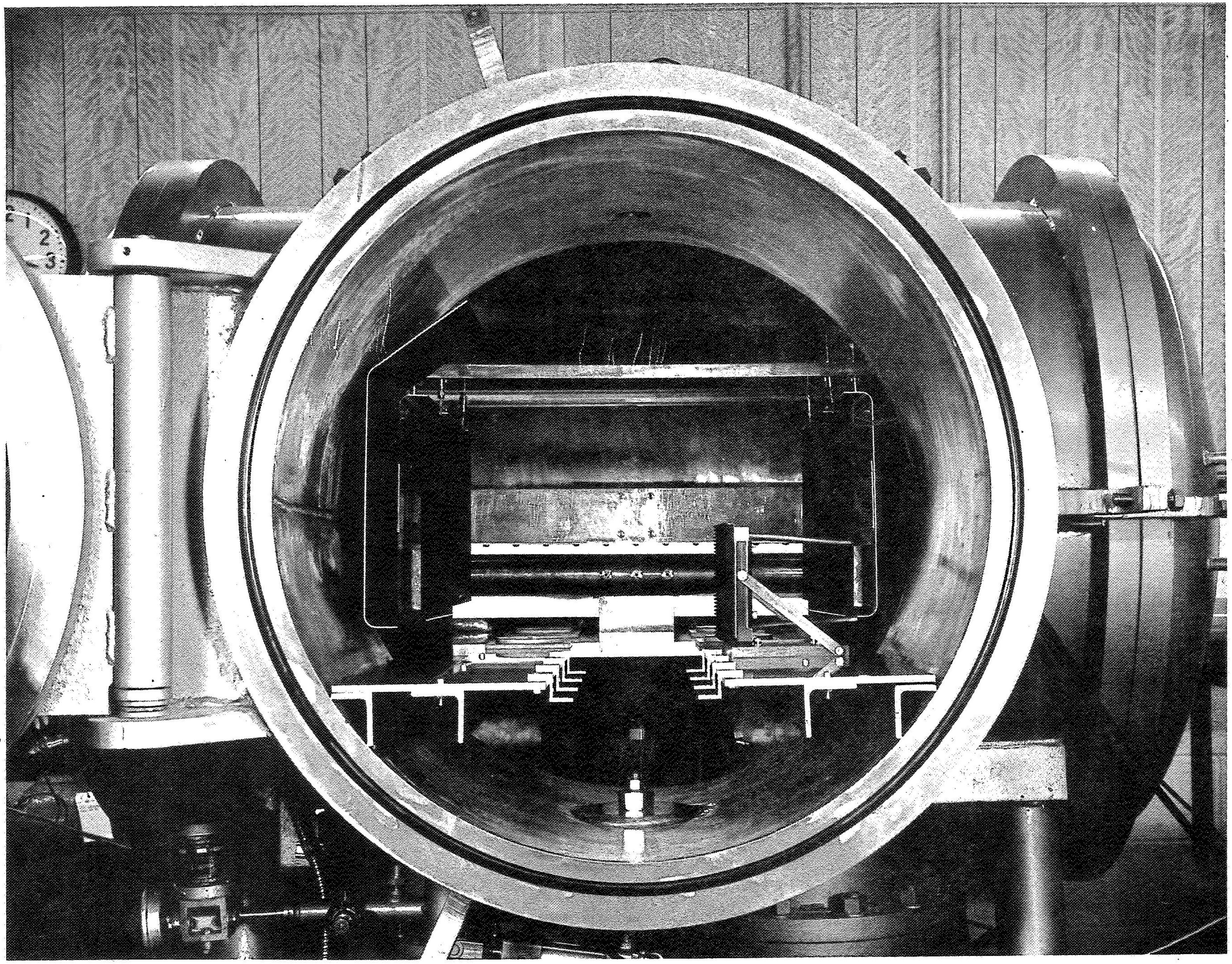

Figure 24 Space Scan and Calibration Targets in Space Chamber

7.0 RADIOMETER PERFORMANCE

Certain parameters affecting system sensitivity are imposed by the satellite orbital characteristics and the mapping geometry. The mapping of contiguous scan lines on the earth's surface or overlying cloud layers is accomplished by continuous rotation of a single-faced scan mirror which makes an angle of 45 degrees to the telescope optical axis. The day-night radiometer operates in much the same fashion as the earlier Nimbus HRIR except that the instantaneous field of view is smaller. The parameters imposed by the satellite characteristics and mapping geometry which affect system sensitivity will be calculated first.

The satellite orbital velocity, v, is given by

$$v = R\sqrt{\frac{g}{R+h}}$$

where g = acceleration of gravity at the earth's surface

R = radius of the earth = 3,440 nautical miles

h = satellite altitude = 750 nautical miles

For $g = 980 \text{ cm/sec}^2 = 5.26 \times 10^{-3}$ nautical miles/sec^2

$$v = 3.85 \frac{\text{nautical miles}}{\text{sec}} = 7.18 \text{ km/sec}$$

In order to obtain contiguous scan lines the period of rotation of the scan mirror, T, must be

$$T = \frac{h\,\phi}{v}\left(1 + \frac{h}{R}\right)$$

where ϕ = width of instantaneous field-of-view.

Using the above values for the various parameters and ϕ= 2.5 milliradians.

$$T = 0.60 \text{ second}$$

The electronic post-demodulation bandwidth, Δf, necessary to record the video signal at this resolution is

$$\Delta f = \frac{\pi}{T\,\phi} = 2100 \text{ hz}$$

The sensitivity of the radiometer is given by the d-c output signal to rms noise ratio which can be written in the following form (modified from Quarterly Report XIII on Contract NAS5-668, Section 3.5).

$$\frac{S_{dc}}{N_{rms}} = \frac{4 \, J_1 (T) \, P_1 (\Delta\lambda, \; T) \, D^* (\Delta\lambda, \; f_c, \; 1) \, T_o \, D_e^2 \, \phi^2}{\pi^2 \qquad\qquad 4 \; \sqrt{\Delta f_s \, A_c}}$$

where $\frac{4}{\pi^2}$ = signal attenuation due to chopping, synchronous demodulation, and electronic filtering (triangular waveform at detector)

$J_1 (T)$ = total source emittance (watts/cm^2) at temperature T

$P_1 (\Delta \lambda T)$ = fraction of blackbody radiation of temperature T in wavelength band $\Delta \lambda$, where $\Delta\lambda$ is the 10.5 to 12.5 micron band

$D^* (\Delta \lambda, f_c, 1)$ = detector detectivity in wavelength band $\Delta\lambda$ for a chopping frequency f_c and electronic bandwidth of 1 cps

T_o = optical transmission (including mirror reflection losses)

D_e = effective optical diameter of collecting telescope

Δf_s = electronic noise bandwidth = $2 \, \Delta f$

A_c = detector cell area.

The effective telescope optical diameter is defined as

$$D_e = \sqrt{D_p^2 - D_s^2}$$

where D_p = diameter of telescope primary mirror

D_s = diameter of telescope secondary mirror

In the breadboard day-night radiometer,

T_o = 0.4

D_e = 3.2 inches

Δf_s = 4.2×10^3 hz

$A_c^{1/2}$ = 5×10^{-2} cm

And the signal-to-noise equation becomes

$$\frac{S_{dc}}{N_{rms}} = 5.166 \times 10^{-6} J_1 P_1 D^*$$

The values of P_1 $(\Delta\lambda, T)$ were determined from the Lowan and Blanch tables (JOSA 40, 70, 1940) for the 10.5 to 12.5 micron band. They are listed in Table 7 together with the values of J_1 (T) and the product J_1 (T) P_1 $(\Delta\lambda, T)$ over the range of expected blackbody temperatures. For a photovoltaic $Cd_x Hg_{1-x} Te$ detector with a maximum response between 10.5 and 12.5 microns, the typical D* is 5 x 10^9 cm $hz^{1/2}$/watt and the best 1 x 10^{10} (See Section 3.0). The signal-to-noise ratio as a function of temperature is shown in Figure 25 for a D* of 5 x 10^9.

Table 7

Blackbody Emittance in the 10.5 to 12.5 Micron Band

T, ^oK	J_1 (T), watts/cm^2	P_1 (10.5 -12.5μ, T)	$J_1 P_1$, watts/cm^2
160	3.715×10^{-3}	4.035×10^{-2}	1.499×10^{-4}
170	4.7345×10^{-3}	5.010×10^{-2}	2.372×10^{-4}
180	5.951×10^{-3}	5.986×10^{-2}	3.562×10^{-4}
190	7.387×10^{-3}	6.951×10^{-2}	5.135×10^{-4}
200	9.070×10^{-3}	7.864×10^{-2}	7.1325×10^{-4}
210	1.102×10^{-2}	8.715×10^{-2}	9.607×10^{-4}
220	1.328×10^{-2}	9.485×10^{-2}	1.2595×10^{-3}
222	1.377×10^{-2}	9.632×10^{-2}	1.3262×10^{-3}
230	1.586×10^{-2}	1.018×10^{-1}	1.6145×10^{-3}
250	2.214×10^{-2}	1.129×10^{-1}	2.501×10^{-3}
270	3.0125×10^{-2}	1.207×10^{-1}	3.636×10^{-3}
290	4.009×10^{-2}	1.254×10^{-1}	5.0265×10^{-3}
310	5.235×10^{-2}	1.275×10^{-1}	6.673×10^{-3}

$\Delta\lambda$ = 10.5 to 12.5 microns
$D^* (\Delta\lambda)$ = 5×10^9 cm hz $^{1/2}$/watt
T_o = 0.4
D_c = 3.2 inches
ϕ = 2.5×10^{-3} radian
$A_c^{1/2}$ = 5×10^{-2} cm
Δf_s = 4.2×10^3 hz

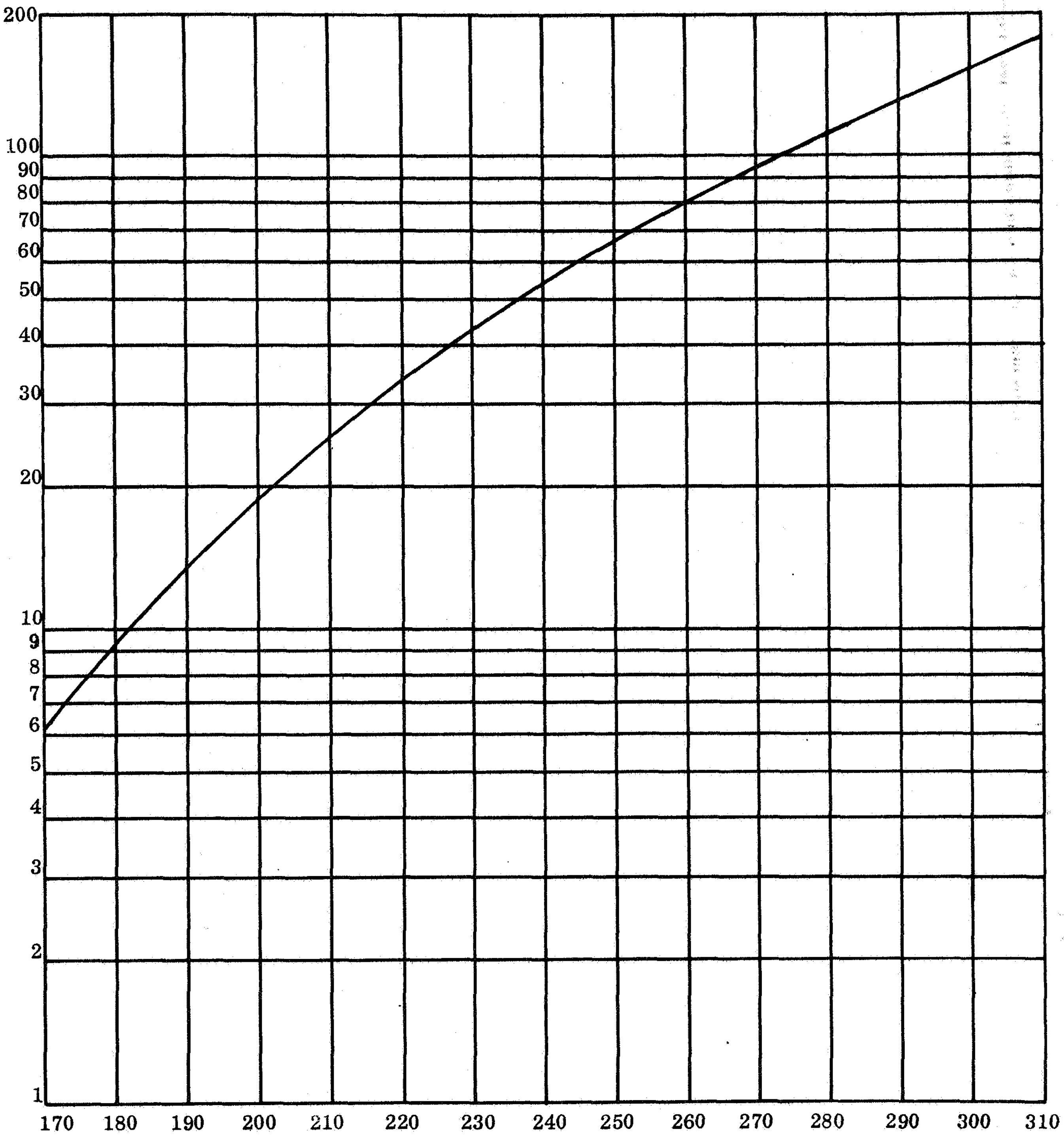

Figure 25 Signal-To-Noise Versus Temperature

The statement of work requires that the noise equivalent temperature be less than 170 degrees K. Figure 25 shows that at 170 degrees K the signal-to-noise ratio is 6.1 for a D* of 5×10^9. The DLK21 photoconductive detector used in the breadboard radiometer has a D* in the spectral band of about 6.9×10^9. The system therefore has a noise equivalent temperature (temperature at which the signal-to-noise is unity) of less than 170 degrees K.

The statement of work also requires that the system must have a noise equivalent temperature difference, ΔT_e, less than 2 degrees K at a target temperature of 220 degrees K. The noise equivalent temperature difference is that temperature change required to produce a change in signal, ΔS, equal to the rms noise. Returning to the signal-to-noise equation we see that

$$\frac{\Delta S}{N_{rms}} = k \, \Delta \left[J_1 (T) \, P_1 (\Delta \lambda, \ T) \right]$$

where Δ denotes a change in the quantity enclosed in the brackets with temperature. For a temperature change from 220 to 222 degrees K

$$\Delta \ J_1 [(T) \, P_1 \, (\Delta \lambda, \ T)] = 6.67 \times 10^{-5} \text{ watts/cm}^2$$

in the 10.5 to 12.5 micron band. The change-in-signal-to-noise ratio for a D* of 5×10^9 is then

$$\frac{\Delta S}{N_{rms}} = 1.7$$

The requirement for a noise equivalent temperature difference of less than 2 degrees K at a blackbody target temperature of 220 degrees K is therefore met.

Since the statement of work permits a telescope diameter of 5 inches, the sensitivity can be improved by increasing the size of the primary optic. The signal-to-noise varies as the square of the effective optical diameter. If the outside diameter of the telescope is increased from 4 to 5 inches with the design unchanged, the signal-to-noise is increased by 1.56 X. The larger collecting aperture can also be used to obtain a smaller instantaneous field-of-view (higher resolution) at the same sensitivity. Including the dependence of the electronic bandwidth on the field-of-view, the signal-to-noise varies as the cube of the field-of-view.

The breadboard radiometer was calibrated in the space chamber at a detector (second-stage patch) temperature of 83 degrees K. The results are shown in Figure 26 for blackbody targets from 180 to 340 degrees K. The 10.5 to 12.5 micron interference filter was mounted in the first-stage patch, which was at a temperature of 103 degrees K.

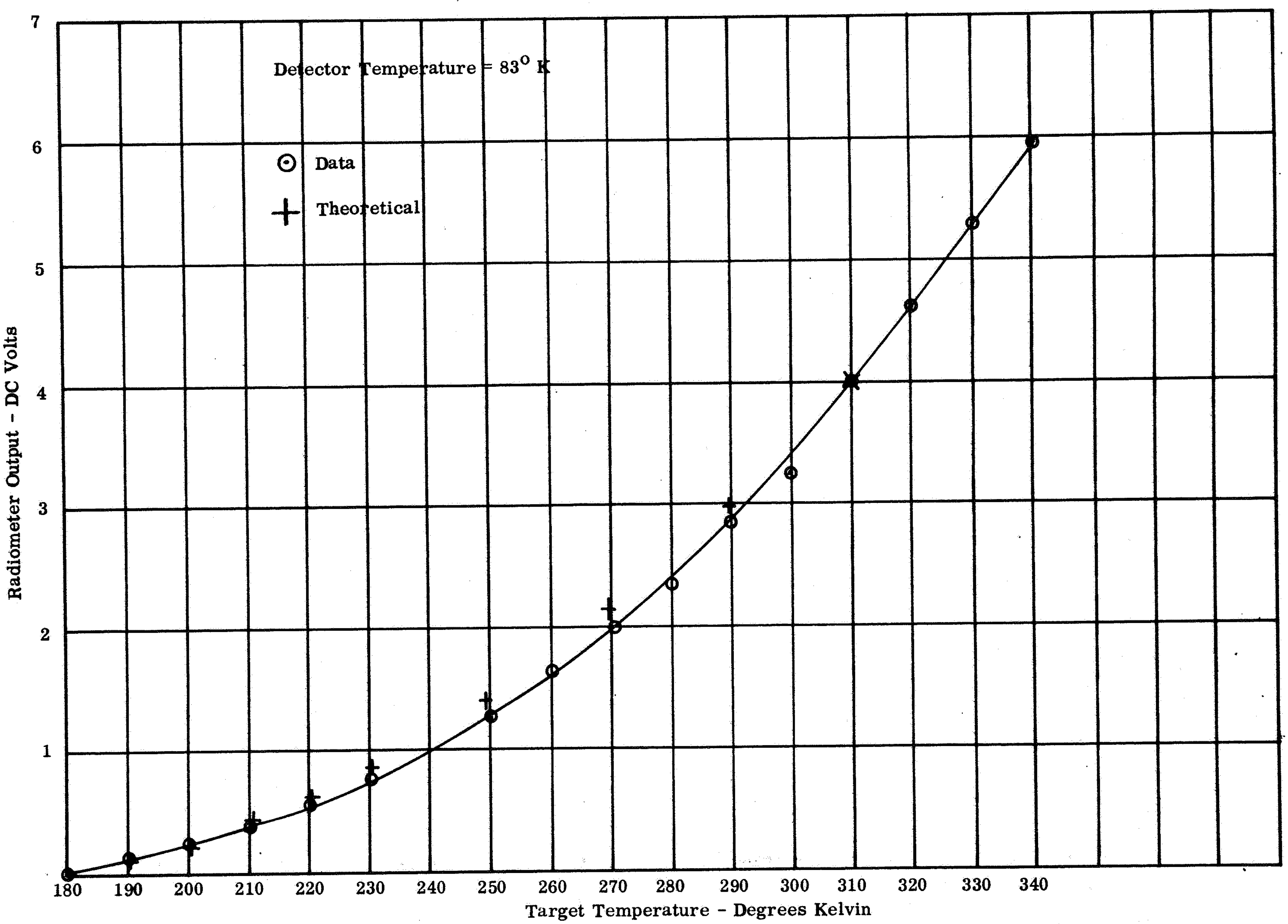

Figure 26 Day-Night Radiometer Calibration

The reference blackbody was at 220 degrees K. This is the temperature of an extension of the aluminum shroud used as a "cold space" scan by the radiometer. In the original data, the output was therefore zero at 220 degrees K and negative for temperatures below 220. The data was modified to a voltage output of zero at 180 degrees K by adding 0. 95 volts (the magnitude of the 180 output) to all the voltages. In this way, the calibration curve shown in Figure 26 was obtained.

A comparison with the theoretical calibration curve was obtained from the data in Table 7. The value of J_1 P_1 at 180 degrees K was subtracted from the J_1 P_1 values over the temperature range of 180 to 310 degrees K. The output (proportional to J_1 P_1) at 310 degrees K was then set at 4. 02 volts (the experimental value), and the theoretical output voltages calculated for 8 temperatures between 180 and 310 degrees K. The results are shown by the crosses in Figure 26. The theoretical points appear to match the experimental data within the accuracy of the temperature measurements on the calibration target; the maximum difference on the temperature scale is about 3 degrees K.

A typical Visicorder tracing of a complete (360 degree) scan line of the radiometer is shown in Figure 27. It shows the reference at 220 degrees K, the radiometer housing, the calibration target at 190 degrees K, and the output produced by the ion gauge at the top of the chamber.

A Reference at 220° K
B Radiometer Housing (Back Scan; Not Black)
C Calibration Target at 190° K
D Ion Gauge

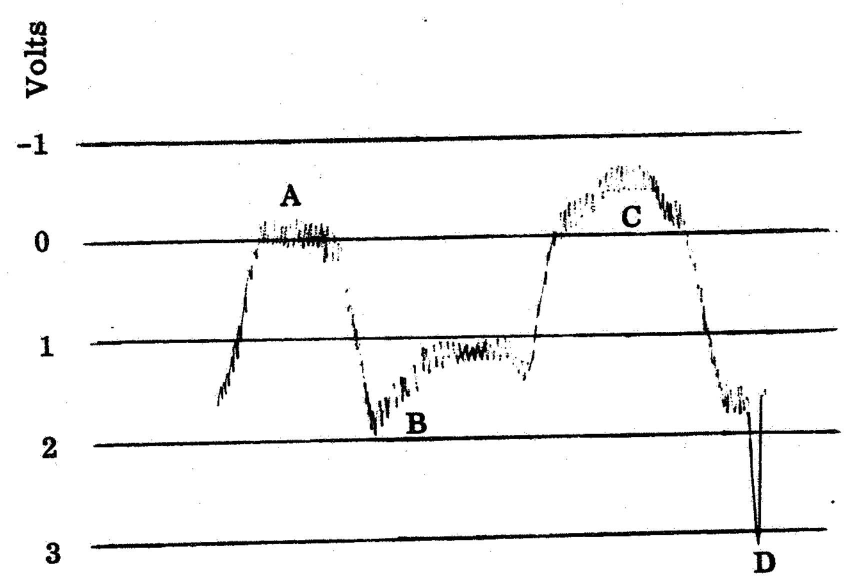

Figure 27 Typical Visicorder Tracing of Radiometer Scan Line

8.0 NEW TECHNOLOGY

No items which are considered new technology according to the NASA new technology clause of September 1964 were developed during the third phase of the contract (breadboard day-night radiometer). However, the breadboard radiometer incorporated the new technology items reported in the first part of the final report (first and second phases of the contract).